Hydrol. Earth Syst. Sci., 28, 4011–4033, 2024
https://doi.org/10.5194/hess-28-4011-2024

Hydrology and Earth System Sciences
Open Access
EGU

Multi-decadal fluctuations in root zone storage capacity through vegetation adaptation to hydro-climatic variability have minor effects on the hydrological response in the Neckar River basin, Germany

Siyuan Wang, Markus Hrachowitz, and Gerrit Schoups

Department of Water Management, Faculty of Civil Engineering and Geosciences, Delft University of Technology, Stevinweg 1, 2628CN Delft, the Netherlands

Correspondence: Siyuan Wang (s.wang-9@tudelft.nl)

Received: 28 February 2024 – Discussion started: 4 March 2024
Revised: 24 June 2024 – Accepted: 14 July 2024 – Published: 3 September 2024

Abstract. Climatic variability can considerably affect catchment-scale root zone storage capacity (S_{umax}), which is a critical factor regulating latent heat fluxes and thus the moisture exchange between land and atmosphere as well as the hydrological response and biogeochemical processes in terrestrial hydrological systems. However, direct quantification of changes in S_{umax} over long time periods and the mechanistic drivers thereof at the catchment scale are missing so far. As a consequence, it remains unclear how climatic variability, such as precipitation regime or canopy water demand, affects S_{umax} and how fluctuations in S_{umax} may influence the partitioning of water fluxes and therefore also affect the hydrological response at the catchment scale. Based on long-term daily hydrological records (1953–2022) in the upper Neckar River basin in Germany, we found that variability in hydro-climatic conditions, with an aridity index I_A (i.e. E_P/P) ranging between ~ 0.9 and 1.1 over multiple consecutive 20-year periods, was accompanied by deviations ΔI_E between -0.02 and 0.01 from the expected I_E inferred from the long-term parametric Budyko curve. Similarly, fluctuations in S_{umax}, ranging between ~ 95 and 115 mm or ~ 20 %, were observed over the same time period. While uncorrelated with long-term mean precipitation and potential evaporation, it was shown that the magnitude of S_{umax} is controlled by the ratio of winter precipitation to summer precipitation ($p < 0.05$). In other words, S_{umax} in the study region does not depend on the overall wetness condition as for example expressed by I_A, but rather on how water supply by precipitation is distributed over the year. However, fluctuations in S_{umax} were found to be uncorrelated with observed changes in ΔI_E. Consequently, replacing a long-term average, time-invariant estimate of S_{umax} with a time-variable, dynamically changing formulation of that parameter in a hydrological model did not result in an improved representation of the long-term partitioning of water fluxes, as expressed by I_E (and fluctuations ΔI_E thereof), or in an improved representation of the shorter-term response dynamics.

Overall, this study provides quantitative mechanistic evidence that S_{umax} changes significantly over multiple decades, reflecting vegetation adaptation to climatic variability. However, this temporal evolution of S_{umax} cannot explain long-term fluctuations in the partitioning of water (and thus latent heat) fluxes as expressed by deviations ΔI_E from the parametric Budyko curve over multiple time periods with different climatic conditions. Similarly, it does not have any significant effects on shorter-term hydrological response characteristics of the upper Neckar catchment. This further suggests that accounting for the temporal evolution of S_{umax} with a time-variable formulation of that parameter in a hydrological model does not improve its ability to reproduce the hydrological response and may therefore be of minor importance for predicting the effects of a changing climate on the hydrological response in the study region over the next decades to come.

Published by Copernicus Publications on behalf of the European Geosciences Union.

1 Introduction

Vegetation is a key component of the terrestrial hydrological cycle as it shapes the hydrological functioning of catchments by regulating the long-term average partitioning of water into drainage and evaporative fluxes (i.e. latent heat), frequently expressed as the runoff ratio $C_r = Q/P$ [–] and evaporative index $I_E = 1 - Q/P = E_A/P$ [–], respectively. More specifically, vegetation transpiration, which despite uncertainties (Coenders-Gerrits et al., 2014) globally constitutes the largest fraction of all evaporative fluxes (Jasechko, 2018), is systematically controlled by the interplay between canopy water demand and water supply from the sub-surface (Donohue et al., 2007; Yang et al., 2016; Jaramillo et al., 2018; Mianabadi et al., 2019). To survive, vegetation needs continuous access to water stored in the sub-surface and access to roots to satisfy its canopy water demand. As a consequence, the vegetation present at any moment, and in particular its active root system, reflects its successful adaptation to the prevalent climatic conditions in a region (Laio et al., 2001; Schenk and Jackson, 2002; Rodriguez-Iturbe et al., 2007; Donohue et al., 2007; Gentine et al., 2012; Liancourt et al., 2012). Irrespective of the geometry, distribution, or structure of root systems, the *maximum* vegetation-accessible water storage volume in the unsaturated root zone of the sub-surface, hereafter referred to as the root zone storage capacity S_{umax} (mm), represents the hydrologically relevant information of root systems (Rodriguez-Iturbe et al., 2007; Nijzink et al., 2016a; Savenije and Hrachowitz, 2017; Gao et al., 2024). Therefore, S_{umax} directly reflects the hydrologically relevant information of root systems at the catchment scales. In response to a changing environment, these root systems of vegetation continuously adapt to allow the most efficient use of available energy and resources for survival. The driving factors of changes in root systems are thus also the driving factors of changes in S_{umax}, as S_{umax} inherently represents adaptations of the root system.

As a central part of hydrological systems, S_{umax} is also a critical parameter in hydrological and land surface models. As such, it can, in principle, be estimated as a function of root depth and the sub-surface pore volume between field capacity and permanent wilting point (Scrivner and Ruppert, 1970; Sivandran and Bras, 2012, 2013). However, these data are typically not available at sufficient levels of detail. Alternatively, catchment-scale S_{umax} can be estimated by three broad approaches. Firstly, it can be obtained by calibration as a parameter of a hydrological model (Nijzink et al., 2018; Bouaziz et al., 2020; Wang et al., 2023; Sriwongsitanon et al., 2023; Roberts et al., 2021; Bahremand and Hosseinalizadeh, 2022; Sadayappan et al., 2023; Tong et al., 2022). Secondly, based on optimality principles, there are some variables like transpiration, nitrogen uptake, or carbon gain that can be maximized to quantify S_{umax} (Guswa, 2008; McMurtrie et al., 2012; Sivandran and Bras, 2012; Yang et al., 2016; Speich et al., 2018). Thirdly, S_{umax} can be robustly estimated at the catchment scale directly from annual water deficits based on observed hydro-climatic data, i.e. precipitation and transpiration (e.g. Donohue et al., 2012; Gentine et al., 2012; Gao et al., 2014b; de Boer-Euser et al., 2016; Nijzink et al., 2016a; Dralle et al., 2021; McCormick et al., 2021; Hrachowitz et al., 2021; Stocker et al., 2023; van Oorschot et al., 2021, 2024). For applications of hydrological and land surface models, S_{umax} (or equivalent parameters) has, except for very few exceptions (Wagener et al., 2003; Merz et al., 2011; Bouaziz et al., 2022; Tempel et al., 2024), been assumed constant over time. As a major knowledge gap, it still remains unknown whether S_{umax} follows climatic variability and evolves over time, thereby reflecting vegetation adaptation to changing conditions.

In contrast, it is well understood that, due to the importance of vegetation for the hydrological functioning of terrestrial systems, anthropogenic land use management practices, such as deforestation and afforestation (Brown et al., 2005; Brath et al., 2006; Fenicia et al., 2009; Alila et al., 2009; Jaramillo et al., 2018; Teuling et al., 2019; Stephens et al., 2021; Hoek van Dijke et al., 2022; Ellison et al., 2024) or irrigation (e.g. AghaKouchak et al., 2015; Van Loon et al., 2016; Roodari et al., 2021), can induce major shifts in the partitioning between the major components of the terrestrial water and energy cycles and thus between I_E and C_r. Two detailed recent studies with well-documented information on deforestation in several experimental catchments could establish explicit mechanistic links between the reduction in S_{umax} by $> 50\,\%$ following deforestation and decreases in I_E (and thus increases in C_r) from ~ 0.4–0.5 to ~ 0.1–0.3, depending on the catchment and the scale of deforestation (Nijzink et al., 2016a; Hrachowitz et al., 2021).

Mapping the shifts to lower I_E that followed these land conversions from forest to grassland- and rangeland-type vegetation as a function of the aridity index $I_A = E_P/P$ in the Budyko framework (Schreiber, 1904; Ol'Dekop, 1911; Budyko, 1974) corresponds well to the results of previous studies that suggest that, across the world, catchments dominated by grass exhibit a consistently lower I_E at the same I_A than forest environments (e.g. Zhang et al., 2001, 2004; Oudin et al., 2008). These differences in the long-term average I_E are accounted for by parametric reformulations of the Budyko framework, such as the Tixeront–Fu equation (Tixeront, 1964; Fu, 1981). The lumped parameters (here: ω) of these expressions define long-term average catchment-specific positions in the I_A–I_E space. As such, the parameters are typically interpreted as encapsulating vegetation characteristics and all other hydro-climatic and physiographic properties of individual catchments besides I_A (e.g. Roderick and Farquhar, 2011; Berghuijs and Woods, 2016). A frequent assumption is that, with changes in climatic conditions, represented here by I_A, individual catchments can be expected to move to the associated new positions I_E, following their specific trajectories defined by ω (e.g. Zhou et al., 2015; Bouaziz et al., 2022). However, several studies have demon-

strated that catchments in many regions worldwide experience deviations ΔI_E from their expected new I_E following a change in I_A (e.g. Jaramillo and Destouni, 2014; van der Velde et al., 2014; Jaramillo et al., 2018; Reaver et al., 2022; Ibrahim et al., 2024; Tempel et al., 2024).

From the above, the following questions arise. (1) Following the notion that vegetation, i.e. individual plants but also the species composition of plant communities, continuously adapts to climatic conditions, does the catchment-scale root zone storage capacity S_{umax} change over multi-decadal timescales? (2) Do multi-decadal changes in the vegetation response, expressed by changes in S_{umax}, explain deviations ΔI_E from the expected I_E? (3) Does a time-variable representation of S_{umax} as a parameter in a hydrological model improve the models' ability to reproduce the hydrological response?

Building on previous studies, the objectives of this study in the upper Neckar River basin in Germany are therefore to provide an analysis of multi-decadal changes in S_{umax} as a result of changing climatic conditions over a 70-year period (1953–2022) and how this further affects hydrological dynamics. More specifically, we test the hypotheses that (1) S_{umax} changes significantly over multiple decades (reflecting vegetation adaptation to climatic variability), (2) changes in S_{umax} affect the long-term partitioning of drainage and evaporation and thus control deviations ΔI_E from the catchment-specific trajectory in the Budyko space, and (3) a time-dynamic implementation of S_{umax} improves the representation of streamflow in a hydrological model.

2 Study area

The upper Neckar River basin in south-western Germany covers an area of $\sim 4000\,km^2$, with the Black Forest on the western side and the Swabian Jura on the south-eastern side. The river basin has a varying topography, with its elevation ranging from 250 m at the outlet in the north to about 1019 m in the south (Fig. 1a, Table 1). Following the elevation gradient, the landscape is dominated by terrace-like elements and undulating hills ($\sim 50\,\%$) with wide valleys used as grasslands and croplands in the lower regions, in particular in the south-eastern parts of the upper Neckar River basin, and by increasingly steep and narrow forested valleys ($\sim 40\,\%$) towards the southern parts and the remaining area that includes flat grassland in valley bottoms ($\sim 10\,\%$) (Fig. 1c). Annual mean precipitation (P) over the whole river basin has a considerable spatial heterogeneity ranging from $\sim 700\,mm\,yr^{-1}$ in the lower parts of the basin to $\sim 1600\,mm\,yr^{-1}$ over the Black Forest, with catchment-average long-term mean precipitation (P) reaching $\sim 880\,mm\,yr^{-1}$ (Fig. 1b, Table 2). The catchment is characterized by a temperate, humid climate with warm, wet summers and cold, drier winters. Precipitation exhibits some seasonality with $\sim 500\,mm\,yr^{-1}$ for the summer months (from May to October) and $\sim 380\,mm\,yr^{-1}$ for the winter months (from November to April), respectively (Fig. 3). Although snow is in general not a major component of precipitation in the study region, snowmelt can have a significant influence during individual storm events. The long-term mean temperature is about 8.2 °C and the potential evaporation (E_P) is about $\sim 860\,mm\,yr^{-1}$, with an aridity index $I_A = E_P/P \sim 0.97$ (Table 2).

3 Data sets

3.1 Data

Daily hydro-meteorological data were available for the period 1 January 1953–31 December 2022 (Fig. 2). Daily precipitation and daily mean air temperature were obtained from stations operated by the German Weather Service (DWD). Precipitation was recorded at 15 stations and temperature measurements were available at 8 stations (Fig. 1) in or close to the study basin. Daily potential evaporation E_P ($mm\,d^{-1}$) was estimated using the Hargreaves equation based on the observed daily maximum and minimum temperatures, has been used in many previous studies, and has been shown to be a suitable method for modelling applications (Oudin et al., 2005). Daily mean discharge data for the period 1 January 1953–31 December 2022 at the outlet of the upper Neckar River basin at Plochingen station were provided by the German Federal Institute of Hydrology (BfG). In addition, data of daily mean discharge for the same time period from three sub-catchments within the upper Neckar River basin (Fig. 1) at the gauges Rottweil (C1; $422\,km^2$), Plochingen at the Fils River (C2; $706\,km^2$), and Horb (C3; $1111\,km^2$) were available from the Environmental Agency of the Baden-Württemberg region (LUBW).

Based on the CORINE Land Cover data set of the upper Neckar River basin during the period 1 January 1953–31 December 2022 (https://land.copernicus.eu/en/products/global-dynamic-land-cover (last access: 27 August 2024), there is only very minor change ($< 2\,\%$) for all the defined land cover classes (Fig. 1c). The 90 m × 90 m digital elevation model of the study region (Fig. 1a) was obtained from the Hydrologic Derivatives for Modeling and Applications (HDMA) database of the United States Geological Survey (USGS) (Verdin, 2017; https://doi.org/10.5066/F7S180ZP) and used to derive the local topographic indices, including height above nearest drainage (HAND) and slope.

3.2 Data pre-processing

For the subsequent experiment (Sect. 4.2), the study basin was stratified into three zones P1–P3 that are characterized by a distinct long-term precipitation pattern (hereafter precipitation zones), following the approach described and implemented for the Neckar River basin by Wang et al. (2023). Briefly, Goovaerts (2000) and Lloyd (2005) showed that areal

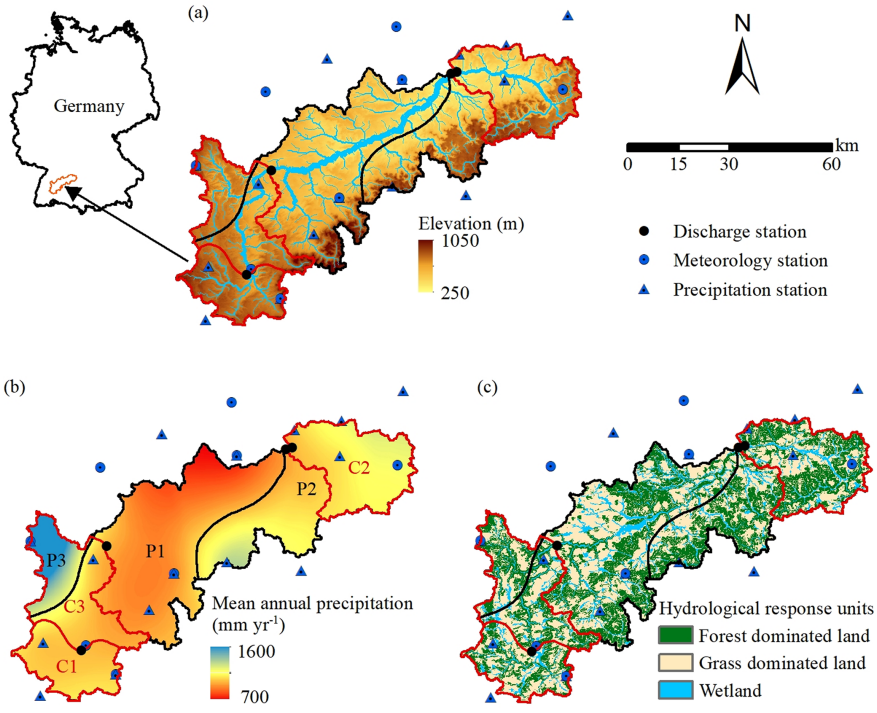

Figure 1. (a) Elevation of the Neckar catchment with discharge and hydro-meteorological stations as well as the water sampling locations used in this study. **(b)** The spatial distribution of long-term mean annual precipitation in the upper Neckar catchment and the stratification into three distinct precipitation zones P1–P3 (black outline), together with the red outlines indicating three sub-catchments (C1: Rottweil; C2: Plochingen at the Fils River; C3: Horb) within the upper Neckar River basin. **(c)** Hydrological response units classified according to their land cover and topographic characteristics.

Table 1. Characteristics of the Neckar catchment in Germany.

Characteristics	
Latitude (N)	48°02′00″–48°46′59″
Longitude (E)	8°18′45″–9°56′33″
Area (km^2)	3968
Average annual precipitation (mm yr^{-1})	880
Average annual temperature (°C)	8.39
Elevation range (m)	250–1019
Mean elevation (m)	554
Slope range (°)	0–53
Mean slope (°)	5.80
Forest-dominated land (%)	39.6
Grass-dominated land (%)	49.6
Wetland (%)	10.8

precipitation estimates informed by elevation data were often more accurate than those based on precipitation gauge observations alone (e.g. Hrachowitz and Weiler, 2011). Thus, to interpolate and estimate areal precipitation across the basin, we used co-kriging that considered elevation, as a preliminary analysis suggested lower errors. Finally, the individual precipitation estimates for each grid cell were used with k-means clustering to establish three clusters representing the three precipitation zones P1–P3 (see Fig. 1b).

To explore the fluctuations of S_{umax} over long timescales, we independently estimate the root zone storage capacity S_{umax} for four subsequent sub-periods of the available data record (t_1–t_4 in Table 2). To survive, root systems of vegetation and the associated vegetation-accessible water storage capacity S_{umax} respond to the ever-changing conditions of their environment. However, as these changes occur at the landscape scale and are mostly reflected in changes in the composition of plant species present in a specific spa-

Table 2. Mean annual precipitation P, potential evaporation E_P, temperature T_M, aridity index I_A, evaporative index I_E, parameter ω for the parametric Budyko framework, root zone storage capacity $S_{umax,WB}$, and $S_{umax,cal}$ based on water balance data and hydrological model calibration for Scenario 1 (entire time period T: 1953–2022) and Scenario 2 (four sub-periods t_1: 1953–1972, t_2: 1973–1992, t_3: 1993–2012, and t_4: 2013–2022).

	Scenario 1	Scenario 2			
	T (1953–2022)	t_1 (1953–1972)	t_2 (1973–1992)	t_3 (1993–2012)	t_4 (2013–2022)
P (mm yr^{-1})	876	870	907	915	811
E_P (mm yr^{-1})	867	836	840	884	906
T_M (°C)	8.4	7.4	7.9	8.7	9.5
I_A [–]	0.97	0.96	0.93	0.97	1.12
I_E [–]	0.57	0.58	0.56	0.56	0.59
ω [–]	1.95	2.01	1.98	1.93	1.89
$S_{umax,WB}$ (mm)	105	95	115	95	100
$S_{umax,cal}$ (mm)	116	98	123	99	107

tial domain, fluctuations in S_{umax} largely occur at timescales that reflect the lifecycles of individual plants. Thus, periods of at least 20 years are required to reflect this and to allow for meaningful estimates of S_{umax}, as also demonstrated by many other studies (e.g. Gao et al., 2014b; Wang-Erlandsson et al., 2016; Singh et al., 2020; Stocker et al., 2023). We therefore had to strike a balance between the number of independent time periods (here: t_1–t_4) and the robustness of the associated S_{umax} estimates. We deliberately chose to emphasize fewer but longer time periods and thus rather reliable estimates of S_{umax}.

4 Methods

To test the hypotheses that the key vegetation parameter, i.e. the root zone storage capacity S_{umax}, evolves over multi-decadal timescales in response to changing hydro-climatic conditions and controls the deviations from expected trajectories in the Budyko space (thereby reflecting the need for time-variable implementations of S_{umax} as a parameter in a hydrological model), the following stepwise approach is designed. (1) Estimate the *observed* deviations ΔI_E from the long-term average expected I_E for four consecutive periods t_1–t_4 in the study period (Table 2). (2) Estimate the root zone storage capacity over the entire study period ($S_{umax,WB,T}$) and the four individual periods t_1–t_4 ($S_{umax,WB,t}$) based on *observed* water balance data. (3) Estimate the root zone storage capacity over the entire study period ($S_{umax,cal,T}$) and the four individual periods t_1–t_4 ($S_{umax,cal,t}$) by *calibration* of a hydrological model over the respective time periods to evaluate whether the changes in the calibrated $S_{umax,cal}$ reflect changes in $S_{umax,WB}$ directly estimated from water balance data from step (2). (4) Estimate the *modelled* deviations ($\Delta I_{E,mT,O'}$) from the expected I_E using both a long-term average time-invariant $S_{umax,WB,T}$ and an individual $S_{umax,WB,t}$ for the four periods t_1–t_4 as model parameters.

4.1 Estimation of the temporal trajectory in the Budyko framework

Mapping aridity $I_A = E_P/P$, where E_P is potential evaporation (mm d^{-1}) and P is precipitation (mm d^{-1}), against the evaporative index $I_E = E_A/P = 1 - Q/P$, where E_A is actual evaporation (mm d^{-1}) and Q is streamflow (mm d^{-1}), the Budyko framework is an expression of the long-term average water balance for a catchment. It is based on the assumption of negligible storage change over the averaging time period, i.e. $dS/dt \sim 0$. As demonstrated by Han et al. (2020), this assumption holds for averaging periods ≥ 10 years for a large majority of catchments worldwide. Note that hereafter the term "evaporation" is used to refer to all combined evaporative fluxes, including interception and soil evaporation (E_i) as well as transpiration (E_T), following the terminology proposed by Savenije (2004) and Miralles et al. (2020).

The analysis in this paper is based on the parametric Tixeront–Fu formulation of the Budyko framework (Tixeront, 1964; Fu, 1981):

$$I_{E,T} = 1 + I_{A,T} - \left(1 + I_{A,T}^{\omega_T}\right)^{1-\omega_T}, \quad (1)$$

where $I_{E,T}$ is the observed evaporative index over a chosen averaging period T, $I_{A,T}$ is the observed aridity index over the same period, and ω_T is the associated catchment-specific parameter that represents all combined catchment properties other than I_A.

In a theoretical catchment that only experiences changes in I_A and no changes in any other hydro-climatic and/or physical catchment characteristics, it can be assumed that ω_T remains constant over time, so that $\omega_T = \omega_{t_i} = \omega_{t_{i+1}}$. This implies that, following a disturbance ΔI_A in a subsequent time period t_{i+1}, the catchment stays on its specific curve defined by ω_T to a new $I_{E t_{i+1}}$. In such a case, ω_T can thus be used to predict future hydrological partitioning I_E. Based on this assumption, here we use the complete available hydro-climatic data record to estimate the long-term average ω_{OT} as

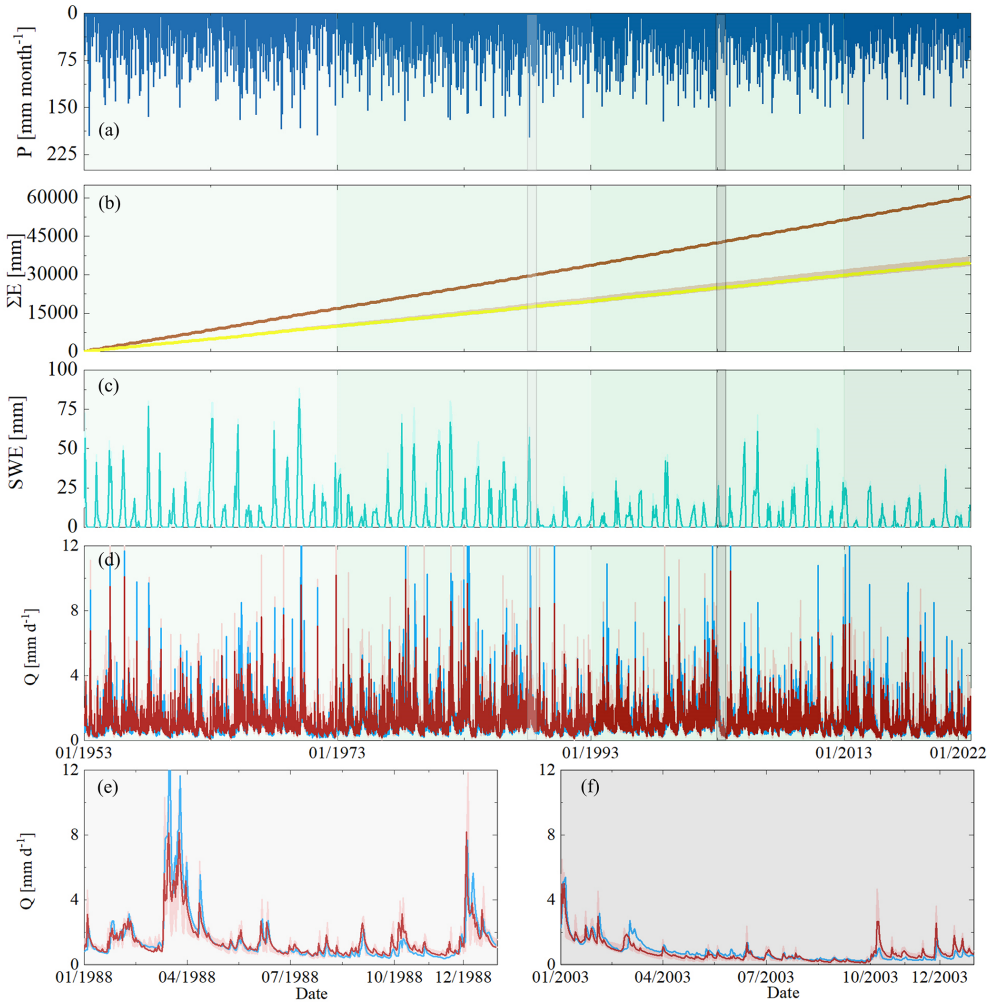

Figure 2. **(a)** Time series of observed monthly precipitation P. **(b)** Daily cumulative evaporative fluxes for the entire time period (1953–2022), where the dark-brown line indicates the potential evaporation E_P and the yellow lines and light-orange-shaded areas show the actual evaporation E_A modelled using the best-fit parameter sets and the associated 5th and 95th percentiles of all feasible solutions calibrated based on the entire time period. **(c)** Monthly maximum values of the snow water equivalent (SWE) for the 1953–2022 time period, where the green line indicates the most balanced solution and the light-green shade indicates the 5th and 95th inter-quantile ranges obtained from all the Pareto optimal solutions calibrated based on the entire time period. **(d)** Observed (blue line) and modelled daily streamflow Q; the red line indicates the most balanced solution and the shaded area indicates the 5th and 95th percentiles of all feasible solutions calibrated based on the entire time period; and the different green background shades from lighter to darker indicate the sub-time periods from t_1 to t_4. Panels **(e)** and **(f)** zoom in to the observed and modelled streamflows for the selected wet year (light-grey shade, 1 January 1988–31 December 1988) and the dry year (grey shade, 1 January 2003–31 December 2003), respectively.

a reference over the entire 1953–2022 study period. The subdivision into the four time periods t_1–t_4 as shown in Table 2 is then allowed to estimate the expected $I_{E,t_i'}$ in the individual periods t_1–t_4: depending on the shift in the observed aridity index along the x axis in t_i ($\Delta I_{A,T,t_i} = I_{A,t_i} - I_{A,T}$), a catchment will move along its parametric Budyko curve defined by ω_{OT} to a new expected position $I_{E,t_i'}$ (Fig. 4).

Based on the available data, we then estimate the individual observed I_{E,t_i} together with the associated ω_{t_i} for each of the four time periods t_1–t_4 (Fig. 5). For each of the four time periods t_1–t_4, the deviation of I_{E,t_i} from the catchment-specific expected $I_{E,t_i'}$, corresponding to a shift from ω_T to $\omega_{t_i} \neq \omega_T$, was then computed as $\Delta I_{E,t_i,t_i'} = I_{E,t_i} - I_{E,t_i'}$.

4.2 Estimation of the root zone storage capacity derived by the water balance method $S_{umax,WB}$

The root zone storage capacity is the *maximum* volume of water which can be held in soil pores of the unsaturated zone and which is accessible to root systems of vegetation for transpiration. Here the water balance method that is described in detail in previous papers (e.g. Gao et al., 2014b; Nijzink et al., 2016a; de Boer-Euser et al., 2016; Wang-Erlandsson

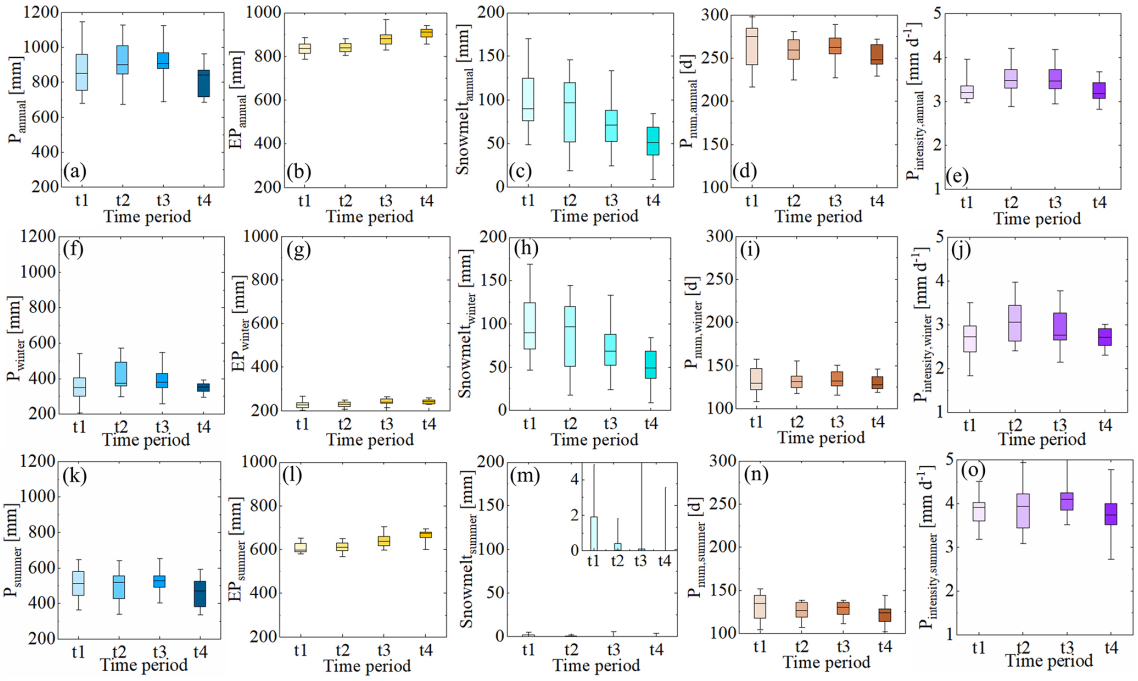

Figure 3. The annual and seasonal variability (i.e. winter and summer) of selected climatic indices, including annual averages of precipitation (P), potential evaporation (E_P), estimated snowmelt water, the number of precipitation days (P_{num}), and the precipitation intensity ($P_{intensity}$) for the four sub-time periods (t_1: 1953–1972, t_2: 1973–1992, t_3: 1993–2012, and t_4: 2013–2022). **(a–e)** The annual variability of selected climatic indices. **(f–j)** The seasonal variability of selected climatic indices in the winter periods. **(k–o)** The seasonal variability of selected climatic indices in the summer periods.

et al., 2016; Bouaziz et al., 2020; Hrachowitz et al., 2021) is used to determine $S_{umax,WB}$. Briefly, $S_{umax,WB}$ is estimated based on daily observations of precipitation (P), potential evaporation (E_P), and streamflow (Q). As a first step, effective precipitation P_e ($mm\,d^{-1}$) that enters the sub-surface is computed by accounting for interception evaporation by

$$P_e(t) = P(t) - E_i(t) - dS_i/dt, \tag{2}$$

where E_i ($mm\,d^{-1}$) is the daily interception evaporation and S_i (mm) is the interception storage. For each time step, E_i is determined by

$$E_i(t) = \begin{cases} E_P(t) & \text{if } E_P dt < S_i, \\ \frac{S_i}{dt} & \text{if } E_P dt \geq S_i. \end{cases} \tag{3}$$

Then, the effective precipitation P_e ($mm\,d^{-1}$) is further estimated according to

$$P_e(t) = \begin{cases} 0 & \text{if } S_i < S_{imax}, \\ \frac{S_i - S_{imax}}{dt} & \text{if } S_i \geq S_{imax}, \end{cases} \tag{4}$$

where S_{imax} (mm) is the maximum interception storage. As S_{umax} is not very sensitive to the choice of S_{imax}, as previously shown by Hrachowitz et al. (2021) and Bouaziz et al. (2022), here we used a value of $S_{imax} = 2$ mm, which was previously also used by de Boer-Euser et al. (2016).

Hereafter, the long-term mean transpiration $\overline{E}_r$ ($mm\,d^{-1}$) is estimated from the long-term water balance, with the assumption of no additional gains or losses:

$$\overline{E}_r = \overline{P}_e - \overline{Q}_O, \tag{5}$$

where $\overline{P}_e$ ($mm\,d^{-1}$) is the long-term mean effective precipitation and $\overline{Q}_O$ ($mm\,d^{-1}$) is the long-term mean observed streamflow. Considering the seasonal fluctuation of energy input, the daily transpiration E_r ($mm\,d^{-1}$) is estimated by subsequently scaling the daily potential evaporation E_P ($mm\,d^{-1}$) minus the interception evaporation E_i ($mm\,d^{-1}$) (see Eqs. 2 and 3) by the long-term mean transpiration $\overline{E}_r$ ($mm\,d^{-1}$), according to (Bouaziz et al., 2022; Hrachowitz et al., 2021)

$$E_r(t) = \frac{\overline{E}_r}{\left(\overline{E}_P - \overline{E}_i\right)}(E_P - E_i), \tag{6}$$

where $\overline{E}_P$ ($mm\,d^{-1}$) is the long-term mean potential evaporation and $\overline{E}_i$ ($mm\,d^{-1}$) is the long-term mean interception evaporation.

From daily storage deficits $S_{rd,n}(t)$ (mm) during dry periods, estimated as the cumulative sum of daily effective precipitation P_e ($mm\,d^{-1}$) minus transpiration E_r ($mm\,d^{-1}$), the maximum storage deficit $S_{rd,n}$ of a specific year n is then computed as follows:

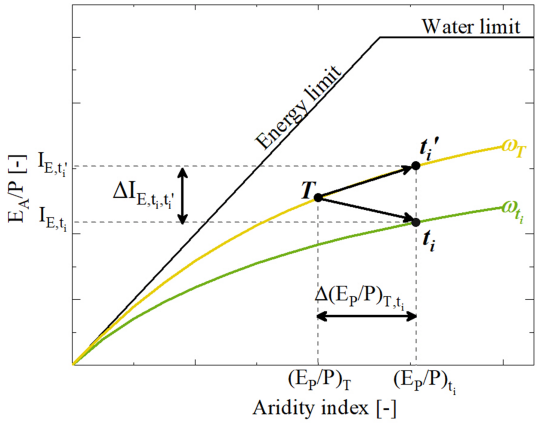

Figure 4. Representation of the Budyko space, which shows the evaporative index ($I_E = 1 - Q/P$) as a function of the aridity index ($I_A = E_P/P$) and the water and energy limits. A catchment with the long-term mean aridity index $I_{A,T} = E_{P,T}/P_T$ and evaporative index $I_{E,T} = 1 - Q_T/P_T$, which is derived from observed data of the entire time period, is plotted at location T on the parametric Budyko curve with ω_T (yellow line) as the baseline. Based on the observed sub-time-period data with the aridity index $I_{A,t_i} = E_{P,t_i}/P_{t_i}$ and evaporative index $I_{E,t_i} = 1 - Q_{t_i}/P_{t_i}$, the same catchment is plotted at location t_i on the parametric Budyko curve with ω_{t_i} (green line). A movement in the Budyko space towards t_i' along the ω_T curve is shown as a result of a change in the aridity index I_{A,t_i} with the assumption that the long-term mean Budyko curve trajectory and the parameter ω are transferable across time for an individual catchment, which results in a significant deviation $\Delta I_{E,t_i,t_i'}$ between the observed evaporative index I_{E,t_i} and the predicted evaporative index $I_{E,t_i'}$.

$$S_{rd,n}(t) = \begin{cases} \int_{t_{0,w}}^{t_{0,d}} (P_e(t) - E_r(t))dt, & \text{if } \int_{t_{0,w}}^{t_{0,d}} (P_e(t) - E_r(t))dt \le 0, \\ 0, & \text{if } \int_{t_{0,w}}^{t_{0,d}} (P_e(t) - E_r(t))dt > 0, \end{cases} \quad (7)$$

$$S_{rd,n} = \max(|S_{rd,n}(t)|). \quad (8)$$

where t is the time step (d), $t_{0,w}$ is the day at the end of the wet period when the storage deficits are zero but $P_e(t) - E_r(t) < 0$, and $t_{0,d}$ is the day when the storage deficits return to zero again after the beginning of the next wet period when the water supply exceeds the canopy water demand, i.e. $(P_e(t) - E_r(t)) > 0$. Any cumulative precipitation surplus is assumed to be drained from the root zone and is released from the system either directly as streamflow or via recharge of the groundwater.

The Gumbel extreme value distribution (Gumbel, 1941) was used previously by several other studies (Gao et al., 2014b; Nijzink et al., 2016a; de Boer-Euser et al., 2016; Bouaziz et al., 2020, 2022; Hrachowitz et al., 2021) to estimate the root zone storage capacity through the water balance approach. Based on fitting the Gumbel distribution to the maximum annual storage deficits for all n years during one of the four time periods t_1–t_4, the root zone storage capacity $S_{umax,WB}$ can be derived from various return periods of the sequence of n maximum annual storage deficits S_{rd}. Previous studies suggested that vegetation develops root zone storage capacities large enough to survive in dry spells with return periods of ∼20–40 years (Gao et al., 2014b; de Boer-Euser et al., 2016; Wang-Erlandsson et al., 2016; Hrachowitz et al., 2021). Therefore, here we define $S_{umax,WB}$ as the maximum storage deficit in a 40-year period so that $S_{umax,WB} = S_{rd,40\ years}$.

Using the above water-balance-based method, we determine $S_{umax,WB}$ for the entire study period 1953–2022 ($S_{umax,WB,T}$) as well as individually for the four time periods t_1–t_4 ($S_{umax,WB,t}$) to quantify potential fluctuations of the root zone storage capacity reflecting the adaptation to changing climatic conditions.

4.3 Hydrological model

4.3.1 Model architecture

Loosely based on the flexible DYNAMITE modular modelling framework (e.g. Hrachowitz et al., 2014), here we used a semi-distributed, process-based model that was previously successfully implemented and tested for the Neckar study basin (Wang et al., 2023) and for many other contrasting environments worldwide (e.g. Prenner et al., 2018; Hulsman et al., 2021a, b; Hanus et al., 2021; Bouaziz et al., 2022). Briefly, this hydrological model consists of three parallel hydrological response units (HRUs), i.e. forest, grassland/cropland, and wetland, which are linked through a common storage component representing the groundwater system (Fig. 5). The classification into the three HRUs was based on the HAND (Gharari et al., 2011) metric and land cover similar to previous studies (e.g. Gao et al., 2014a; Gharari et al., 2014; Nijzink et al., 2016b; Bouaziz et al., 2021). The model was further spatially discretized by stratification into 100 m elevation bands for a more detailed representation of the snow storage (S_{snow}) and was finally implemented in parallel, i.e. individually for each of the three precipitation zones P1–P3, to balance to a certain degree spatial differences in precipitation with computational requirements. Rain (P_{rain}) and meltwater (M_{snow}) from the different elevation zones were aggregated according to their associated spatial weights in each elevation zone as further input to the subsequent layers of the model in each HRU. The outflows from each HRU in each precipitation zone and finally the outflows from each precipitation zone were likewise aggregated according to their respective spatial weights to represent the catchment-aggregated outflows. While the three HRUs are characterized by distinct parameters that reflect their respective functioning, the parameters between the individual zones P1–P3 were, in the spirit of model parsimony, kept the same in what is elsewhere referred to as a distributed moisture-accounting approach (e.g. Ajami et al., 2004; Fenicia et al.,

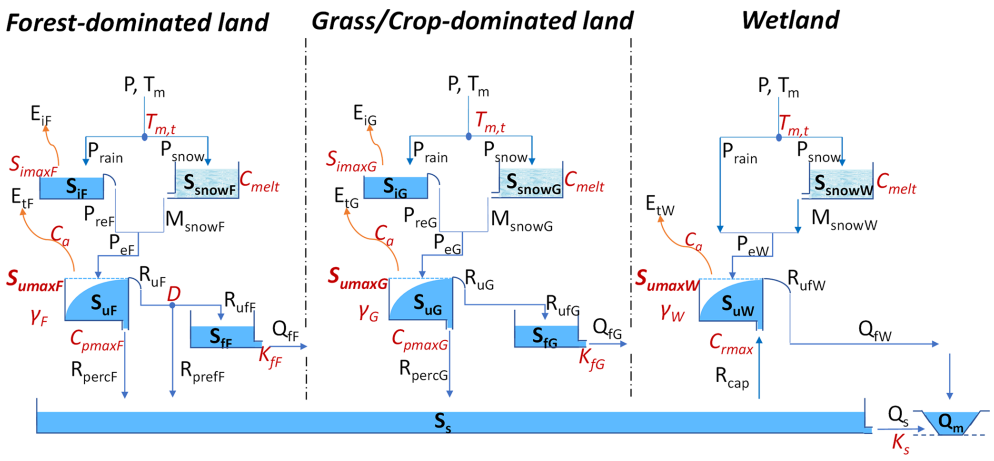

Figure 5. Model structure of the distributed conceptual hydrological model, discretized into three parallel hydrological response units (HRUs), i.e. forest, grassland, and wetland in each precipitation zone from P1 to P3. The light-blue boxes indicate the hydrologically active individual storage volumes. The arrow lines indicate water fluxes and the model parameters are shown in red. All the symbols are described in Table S1 in the Supplement.

Table 3. Flow signatures and the associated performance metrics used for model calibration and evaluation. The performance metrics include the Nash–Sutcliffe efficiency (NSE) and the relative error (RE).

Signature	Symbol	Performance metric
Time series of streamflow	Q	$\mathrm{NSE_Q}$
Time series of $\log(Q)$	$\log(Q)$	$\mathrm{NSE_{\log(Q)}}$
Flow duration curve of $\log(Q)$	$\mathrm{FDC_{\log(Q)}}$	$\mathrm{NSE_{FDC\,\log(Q)}}$
Seasonal runoff coefficient	C_r	$\mathrm{NSE}_{C_\mathrm{r}}$
Autocorrelation function of flow (AC)	AC	$\mathrm{NSE_{AC}}$
Runoff coefficient in summer	$C_\mathrm{r,summer}$	$\mathrm{RE}_{C_\mathrm{r,summer}}$
Runoff coefficient in winter	$C_\mathrm{r,winter}$	$\mathrm{RE}_{C_\mathrm{r,winter}}$

2008; Euser et al., 2015). Overall, the model consists of snow (S_snow), interception (S_i), the unsaturated root zone (S_u), and fast-responding (S_f) and slow-responding storage (S_s) components for each HRU and precipitation zone. The maximum storage volume in the unsaturated root zone component in each HRU is defined by the corresponding calibration parameters $S_\mathrm{umax,F}$, $S_\mathrm{umax,G}$, and $S_\mathrm{umax,W}$, respectively. The catchment average $S_\mathrm{umax,cal}$ is then inferred by aggregating these parameters according to their spatial weights. Water can be released from unsaturated root zones as the combined soil evaporation and transpiration flux E_t ($\mathrm{mm\,d^{-1}}$), which is a frequently applied way of representing vegetation water stress (e.g. Bouaziz et al., 2021; Gharari et al., 2013; Gao et al., 2014a). The equations of the model are provided in Table S1 in the Supplement, and more detailed descriptions of the model are provided by Wang et al. (2023) and the other earlier implementations referred to above.

4.3.2 Model calibration

The model was run with a daily time step and has 18 calibration parameters. Briefly, the model parameters were calibrated by using the Borg_MOEA algorithm (Borg Multi-objective evolutionary algorithm; Hadka and Reed, 2013) and were based on uniform prior distributions (Table S2 in the Supplement). To best reflect different aspects of the hydrograph (including high flows, low flows, and the partitioning of precipitation into runoff and evaporation), the parameters were calibrated using a multi-criteria approach that includes seven objective functions as performance metrics $E_{\mathrm{Q},n}$ (Table 3). There are multiple ways of dealing with sets of Pareto front solutions, as described in detail by e.g. Efstratiadis and Koutsoyiannis (2010) or Gharari et al. (2013). We chose to use all solutions on the Pareto front to obtain a conservative estimate of uncertainty. The seven performance metrics were subsequently also combined into an overall performance metric based on the Euclidian distance (D_E), where $D_\mathrm{E} = 1$ indicates a perfect fit. To find a somewhat balanced solution in the absence of more detailed information, all individual performance metrics were equally weighted here (e.g. Hrachowitz et al., 2021; Hulsman et al., 2021b; Wang et al.,

2023):

$$D_{\mathrm{E}} = 1 - \sqrt{\frac{\sum_{n=1}^{N}(1 - E_{\mathrm{Q},n})^2}{N}}, \quad (9)$$

where $N = 7$ is the number of performance metrics with respect to streamflow ($E_{\mathrm{Q},n}$). Note that the different units and thus different magnitudes of residuals in the individual performance metrics introduce some subjectivity in finding the most balanced overall solution according to D_{E} (Eq. 9). However, a preliminary sensitivity analysis with varying weights for the individual performance metrics in D_{E} suggested limited influence on the overall results and is thus not further reported here. In addition, the model was tested for its ability to represent spatial differences in the hydrological response by evaluating it against streamflow observations in three sub-catchments (C1–C3) of the upper Neckar catchment without further recalibration, where each one of the sub-catchments largely represents the hydrological response from one of the precipitation zones (Fig. 1).

The model is calibrated following two distinct calibration scenarios as indicated in Table 2. In the first scenario, the model and thus also $S_{\mathrm{umax,F}}$, $S_{\mathrm{umax,G}}$, and $S_{\mathrm{umax,W}}$ are calibrated over the full length of the 70-year study period from 1953 to 2022. This reflects the common assumption of a system that is stable over time. By extension, this also implies that the role of vegetation and thus S_{umax} does not change and that vegetation does not adapt to climatic variability. In the second scenario, individual calibration to the four time periods t_1–t_4 allowed us to estimate fluctuations in the parameters $S_{\mathrm{umax,F}}$, $S_{\mathrm{umax,G}}$, and $S_{\mathrm{umax,W}}$ between the time periods as an indicator of vegetation adaptation to changing climatic conditions.

5 Results

5.1 Observed multi-decadal hydro-climatic variability

Based on the initial analysis of water balance data for the four sub-time periods, significant differences were observed in the variability of different hydro-climatic indicators over the 1953–2022 study period (Fig. 3). While periods t_1 and t_4 were characterized by rather low mean annual precipitation of ~ 870 and $811\,\mathrm{mm\,yr^{-1}}$, respectively, periods t_2 and t_3 were subject to, on average, higher precipitation of $\sim 911\,\mathrm{mm\,yr^{-1}}$. While summer precipitation remained rather stable over the study period (Fig. 3f), the above was mostly caused by fluctuations in winter precipitation (Fig. 3k). In contrast, potential evaporation E_{P} has gradually increased by 7 % from 836 to $906\,\mathrm{mm\,yr^{-1}}$ (Fig. 3b). Similarly reflecting increases in temperature (Fig. 3b), the annual snowpack and associated snowmelt have continuously decreased from around $98\,\mathrm{mm\,yr^{-1}}$ to around $50\,\mathrm{mm\,yr^{-1}}$ between t_1 and t_4 (Fig. 3c). A slight decrease in the number of days with precipitation from ~ 264 to 251 (Fig. 3d), on average, mostly due to changes in the summer months (Fig. 3n), was accompanied by some rather limited variability in precipitation intensities (Fig. 3e), mostly during winter (Fig. 3j). Overall, the comparatively humid periods t_1–t_3 that were characterized by I_{A} fluctuating between 0.93 and 0.97 were followed by a markedly more arid period t_4 with $I_{\mathrm{A}} = 1.12$ (Table 2, Fig. 6). In response to the multi-decadal variability in I_{A}, expressed as movement along the x axis in the Budyko framework, the catchment experienced I_{E} varying between 0.56 and 0.59 (Table 2, Fig. 6). However, this observed variability was somewhat lower than the variability $I_{\mathrm{E},\omega\mathrm{T}} = 0.55$–0.61 that would have been expected based on ω_{T}. This illustrates that the hydrological response did not consistently follow its long-term trajectory defined by ω_{T}. Instead, deviations $\Delta I_{\mathrm{E},t_i}$ from the expected positions, and thus values of ω_{t_i} that are different to ω_{T}, were observed for the individual periods. More specifically, the deviations gradually decreased from $\Delta I_{\mathrm{E},t_1} = 0.01$ in t_1 to $\Delta I_{\mathrm{E},t_4} = -0.02$ in t_4 (Fig. 6). This systematic shift towards lower (more negative) $\Delta I_{\mathrm{E},t_i}$ and thus also lower ω_{t_i} indicates that, at the same I_{A}, a smaller fraction of precipitation is released as evaporation, i.e. I_{E}, now than at the start of the 70-year study period. Although the magnitude of deviations of $\Delta I_{\mathrm{E},t_i} \leq \pm 0.02$ remains rather minor, similar to what was recently reported elsewhere (Ibrahim et al., 2024; Tempel et al., 2024), their systematic shift in particular to one direction implies that changes in the system other than I_{A} have a visible effect on the hydrological response pattern.

5.2 Root zone storage capacity $S_{\mathrm{umax,WB}}$ estimated from water balance data

As the baseline of our study, the annual maximum storage deficits fluctuate between 97 mm in 2022 and 16 mm in 1970 (Fig. 7a). Assuming an adaptation to dry spells with 40-year return periods, the root zone storage capacity over the entire 1953–2022 study period (Scenario 1) was estimated to be $S_{\mathrm{umax,WB,T}} = 105$ mm (Table 2, Fig. 7b). In the next step, the storage deficits and the associated root zone storage capacity for each period from t_1 to t_4 were estimated (Scenario 2). $S_{\mathrm{umax,WB,t1}}$ and $S_{\mathrm{umax,WB,t3}}$ for periods t_1 and t_3, respectively, are estimated at the same value of 95 mm. In contrast, and somewhat counterintuitively, the highest value over the study period is found in the wettest period (t_2) and reaches $S_{\mathrm{umax,WB,t2}} = 115$ mm, while the driest period (t_4) is characterized by $S_{\mathrm{umax,WB,t4}} = 100$ mm (Table 2, Fig. 7c–j). These patterns suggest that $S_{\mathrm{umax,WB}}$ did vary by ~ 20 mm, equivalent to ~ 20 % throughout the 1953–2022 period. In contrast to $\Delta I_{\mathrm{E},t_i}$, which was characterized by a systematic shift towards more negative deviations over time, no evidence was found of a systematic, one-directional shift in $S_{\mathrm{umax,WB}}$. Instead, $S_{\mathrm{umax,WB}}$ evolved following a somewhat cyclic pattern.

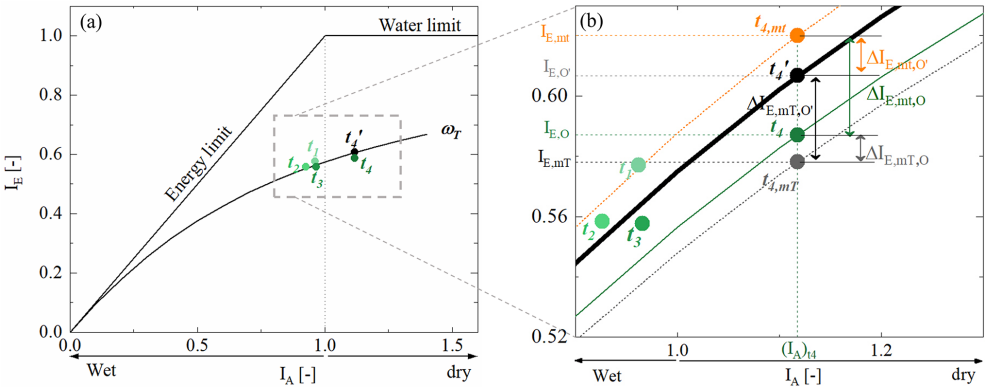

Figure 6. (a) Green dots from the light dot to the dark dot indicate the observed positions for the four sub-time periods t_1–t_4. The black dot t_4' indicates the expected location on the parametric Budyko curve with ω_T derived from the entire observed time period. We select time period t_4 as an example to present the modelled positions in the zoom-in plot **(b)**. The grey dot $t_{4,mT}$ indicates the modelled position based on Scenario 1, which is with $S_{umax,WB,T}$, and the orange dot $t_{4,mt}$ indicates the modelled position based on Scenario 2, which is with $S_{umax,WB,t4}$. $\Delta I_{E,mT,O'}$ (black arrow) indicates the deviation between the modelled $I_{E,mT}$ based on Scenario 1 and the expected $I_{E,O'}$. $\Delta I_{E,mt,O'}$ (orange arrow) indicates the deviation between the modelled $I_{E,mt}$ based on Scenario 2 and the expected $I_{E,O'}$. $\Delta I_{E,mT,O}$ (grey arrow) indicates the deviation between the modelled $I_{E,mT}$ based on Scenario 1 and the observed $I_{E,O}$. $\Delta I_{E,mt,O}$ (green arrow) indicates the deviation between the modelled $I_{E,mt}$ based on Scenario 2 and the observed $I_{E,O}$.

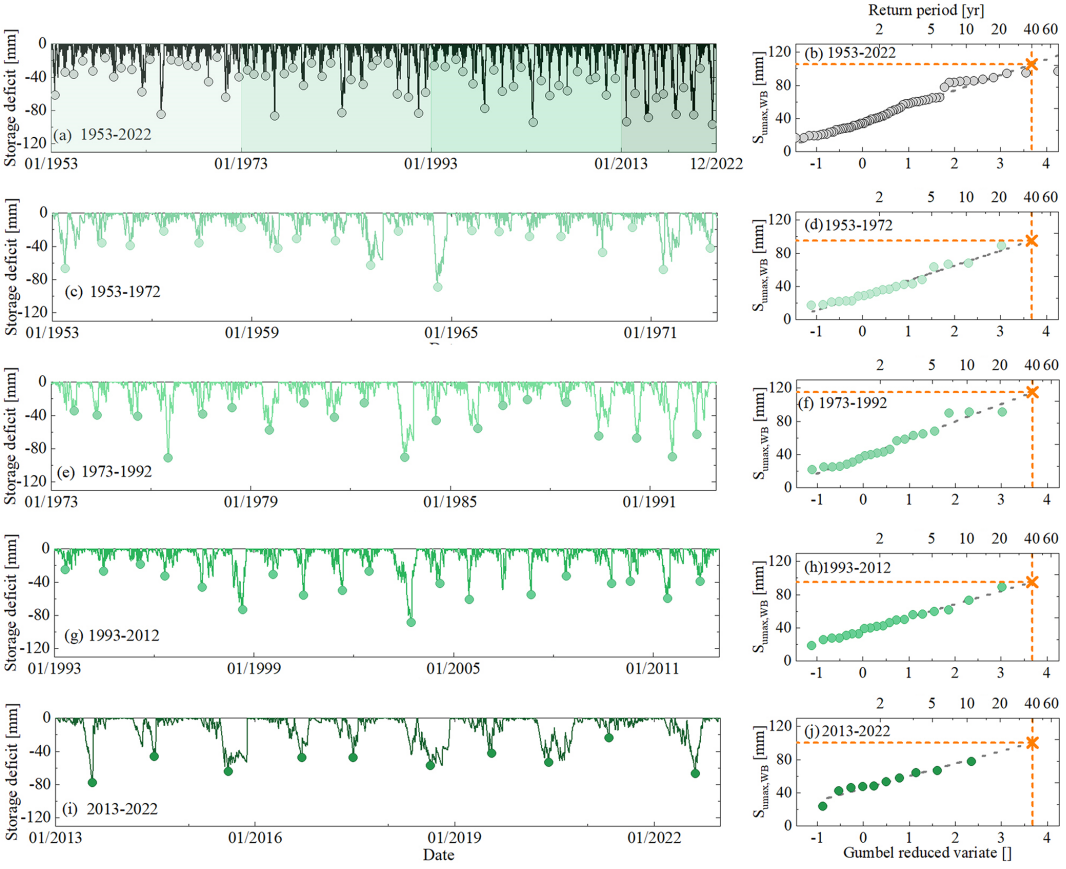

Figure 7. The time series of storage deficits as calculated by Eq. (7) for the entire time period T (1953–2022) and for the four sub-time periods (green shades from light to dark for the time period from t_1 to t_4) (**a**, **c**, **e**, **g**, and **i**). The maximum annual deficits are indicated by the dots. Estimation of S_{umax} as the storage deficit associated with a 40-year return period using the Gumble extreme value distribution for different time periods (**b**, **d**, **f**, **h**, and **j**). The orange crosses indicate the values of S_{umax} for the different time periods.

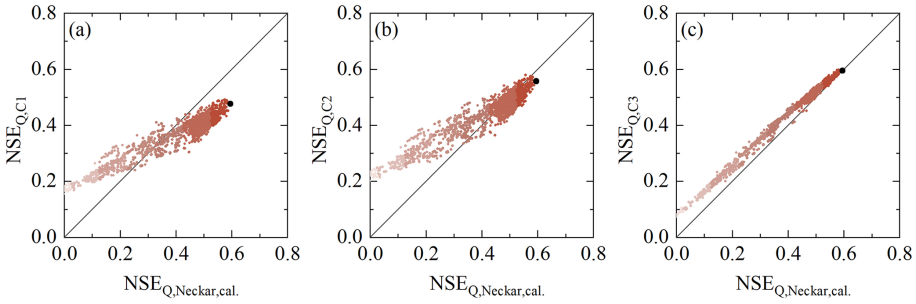

Figure 8. Selected model performance metrics in the entire time period 1 January 1953–31 December 2022 of the upper Neckar River basin against the model performance in uncalibrated sub-catchment-based (C1: Rottweil; C2: Plochingen at the Fils River; C3: Horb) parameter sets derived from the calibration for the entire time period. The dots indicate all the Pareto optimal solutions in the multi-objective model performance space. The shades from dark to light indicate the overall model performance based on the Euclidean distance D_E, with the black solutions representing the overall better solutions (i.e. larger D_E).

5.3 Root zone storage capacity $S_{umax,cal}$ estimated as a calibration parameter

5.3.1 Model calibration for 1953–2022 (Scenario 1)

The model parameter sets determined as feasible after calibration over the entire 1953–2022 study period in Scenario 1 reproduce the main features of the hydrological response (Fig. 2d). More specifically, the modelled hydrographs in particular describe the timing of high flows well while somewhat underestimating the flow peaks for the best-performing model in terms of D_E (Eq. 9). The low flows and the shapes of the recessions are generally captured well ($NSE_{\log Q} = 0.67$). Crucially, the model also reproduces the other observed streamflow signatures well, e.g. the flow duration curves ($NSE_{\log FDC} = 0.96$), the autocorrelation function ($NSE_{AC} = 0.99$), and the long-term and seasonal runoff coefficients ($NSE_{C_r} = 0.90$, $RE_{C_r,summer} = 0.83$, and $RE_{C_r,winter} = 0.91$). The latter further implies that the modelled long-term actual evaporative fluxes E_A (Fig. 2b) and thus $I_{E,\omega T}$ are, on average, consistent with the observed ones, which can be seen in Fig. 6. The model, calibrated on the overall response of the upper Neckar River basin, also exhibited considerable skill in representing spatial differences in the hydrological response by reproducing observed streamflow in the three sub-catchments (C1–C3) similarly well (Fig. 8) without any further recalibration. The overall model skill to mimic the hydrological response corresponds well to a similar implementation of the model in the greater study area by Wang et al. (2023). A detailed list of the performance metrics is provided in Table S4 in the Supplement.

The model calibration resulted in pronounced differences in the root zone storage capacity parameters for three individual landscape classes. While for forest-dominated land it was estimated at $S_{umax,F} = 158$ mm for the best-performing model (5th and 95th percentiles of all feasible solutions: 138–168 mm), it reached $S_{umax,G} = 95$ mm (5th and 95th percentiles: 71–123 mm) for grassland/cropland and $S_{umax,W} = 61$ mm for wetland (5th and 95th percentiles: 49–68 mm), which reflects differences in the vegetation type and position in the landscape (Fan et al., 2017). Remarkably, the catchment root zone storage capacity, estimated by aggregating the individual values according to their areal fractions, at $S_{umax,cal} = 116$ mm (5th and 95th percentiles: 99–130 mm; Fig. 9a) came very close to the estimate of $S_{umax,WB} = 105$ mm that is directly derived from the water balance method without any calibration, as described in Sect. 5.2.

5.3.2 Model calibration for the individual periods t_1–t_4 (Scenario 2)

The model parameter sets obtained from the individual calibration for each period from t_1 to t_4 reproduce the hydrographs of the corresponding periods as well or slightly better than when using the long-term average parameters from Scenario 1 (see the detailed performance metrics in Table S4). In particular, the runoff coefficients of $NSE_{C_r} \sim 0.86$–0.91, $RE_{C_r,summer} \sim 0.84$–$0.90$, and $RE_{C_r,winter} \sim 0.88$–$0.92$ could be mimicked rather well. Similarly, the daily dynamics with $NSE_{\log Q} \sim 0.63$–0.72 for the best-performing model of each period and most other hydrological signatures could be reproduced marginally better.

The individual calibration over each period t_1–t_4 resulted in associated differences in the catchment-scale root zone storage capacity of each period. Based on the best-performing models, the calibrated values varied between low values for t_1 and t_2, with $S_{umax,cal,t_1} = 98$ mm and $S_{umax,cal,t_3} = 99$ mm, and higher values for the other two periods, with $S_{umax,cal,t_2} = 122$ mm and $S_{umax,cal,t_4} = 107$ mm (Table 2, Fig. 9a). The magnitudes of S_{umax,cal,t_i} obtained by calibration in the individual time periods t_1–t_4 are, with a difference of 5 mm ($\sim 5\,\%$), on average very close to the S_{umax,WB,t_i} estimated on the basis of the water balance for the same periods. Perhaps even more notably, the temporal

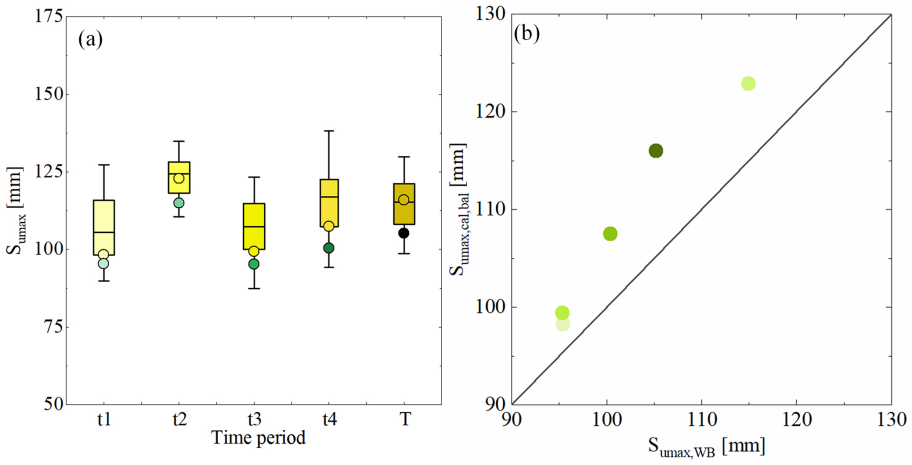

Figure 9. (a) S_{umax} values derived from the water balance method and the hydrological model for different time periods. The yellow boxes from light to dark indicate the range of $S_{umax,cal}$ for the sub-time period from t_1 to t_4 and the entire time period T based on the corresponding parameter sets derived from the model. Yellow dots indicate the corresponding $S_{umax,cal,bal}$ based on the most balanced solution, and green dots indicate the corresponding $S_{umax,WB}$ derived from the water balance method. **(b)** Values of $S_{umax,cal,bal}$ against $S_{umax,WB}$. The yellow–green dots from light to dark indicate the values of S_{umax} for the sub-time period from t_1 to t_4 and the entire time period T.

evolution of S_{umax,cal,t_i} and S_{umax,WB,t_i} follows the same sequence over time ($R^2 = 0.95$, $p = 0.05$; Fig. 9b).

5.4 Effect of S_{umax} on temporal fluctuation in the trajectories of the Budyko curve

The deviations $\Delta I_{E,O,O'}$ between the expected evaporative index $I_{E,O'}$ and the observed evaporative index $I_{E,O}$ for all the periods t_1–t_4 become gradually more negative from t_1 ($\Delta I_{E,O,O'} = 0.013$) to t_4 ($\Delta I_{E,O,O'} = -0.020$), which is consistent with decreases in ω_{t_i} and downward shifts of the associated parametric Budyko curves over time as described in Sect. 5.1. These systematic reductions in $\Delta I_{E,O,O'}$ over the 70-year study period are not reflected in the fluctuations of root zone storage capacities, irrespective of how they were estimated, i.e. S_{umax,WB,t_i} ($p = 0.85$) or S_{umax,cal,t_i} ($p = 0.96$), as illustrated in Fig. 10.

The above is further corroborated by comparing the modelled I_E from Scenarios 1 and 2 for each period t_1–t_4. More specifically, in Fig. 11c it can be seen that Scenario 1, based on a time-invariant, long-term average $S_{umax,WB,T}$ obtained over the entire 1953–2022 period generates deviations $\Delta I_{E,mT,O'}$ from the expected long-term average $I_{E,O'}$ for each period t_1–t_4. In this case, the modelled I_E does not follow the expected $I_{E,O'}$. However, nor does it follow the sequence of increasingly negative deviations from 0.013 in t_1 to −0.020 in t_4 as observed in reality ($\Delta I_{E,O,O'}$). Instead, $\Delta I_{E,mT,O'}$ remains negative for all the time periods and fluctuates between $\Delta I_{E,mT,O'} = -0.005$ and −0.029 (white boxplots in Fig. 11c). Replacing the time-invariant $S_{umax,WB,T}$ with an individual S_{umax,WB,t_i} for each period t_1–t_4 in Scenario 2 accounts for the different effects of vegetation in the individual periods. If S_{umax} controlled the observed deviations from the expected $I_{E,O'}$, Scenario 2 would generate estimates of $\Delta I_{E,mt_i,O'}$ that are closer to the observed ones than those of Scenario 1. However, no evidence was found of that: the deviations $\Delta I_{E,mt,O'}$ obtained by Scenario 2 with time-variable S_{umax} for each period t_1–t_4 are largely indistinguishable (orange boxplots in Fig. 11c) from those generated by Scenario 1 with time-invariant S_{umax}. As a consequence, the evaporative index I_E modelled with time-variable S_{umax,WB,t_i} is not found to be closer to the observed I_E for Scenario 2 than for Scenario 1. On the contrary, the deviations $\Delta I_{E,m,O}$

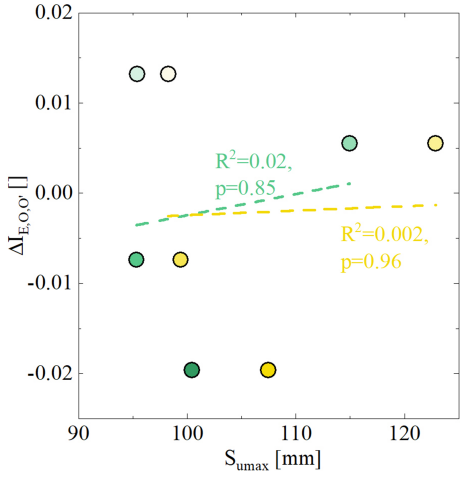

Figure 10. Relationships between the deviations $\Delta I_{E,O,O'}$ and the values of $S_{umax,WB}$ and $S_{umax,cal}$ for the four sub-time periods (t_1–t_4) which are derived from the water balance method (green circles) and the hydrological model calibration (yellow circles), respectively.

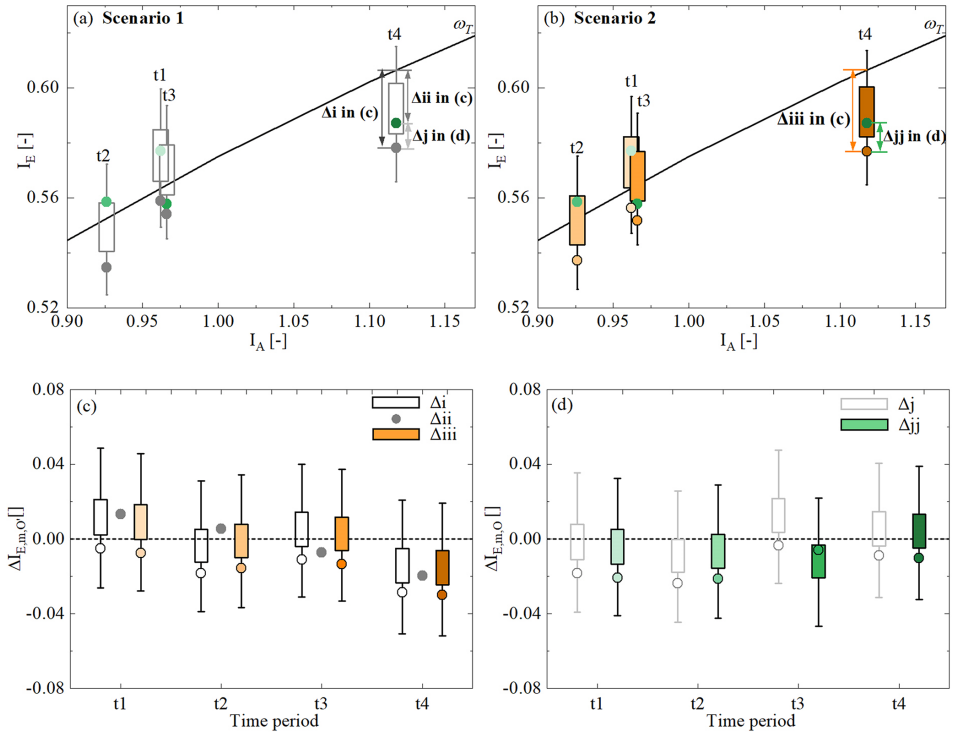

Figure 11. **(a)** The grey boxes ($I_{E,mT}$) indicate the modelled evaporative index based on all the Pareto front solutions for the four sub-time periods based on Scenario 1 with a stationary $S_{umax,WB,T}$ and grey dots based on the most balanced solution based on Scenario 1. The green circles from light to dark in panels **(a)** and **(b)** indicate the observed evaporative index for the four sub-time periods from t_1 to t_4. **(b)** The orange circles ($I_{E,mt}$) indicate the modelled evaporative index based on all the Pareto front solutions for the four sub-time periods (from lighter to darker shades) based on Scenario 2 with time-variant S_{umax,WB,t_i} and the orange circles based on the most balanced solution for Scenario 2. The black boxes in panel **(c)** indicate the deviations $\Delta I_{E,mT,O'} = I_{E,mT} - I_{E,O'}$ (Δ i) based on all the Pareto front solutions for the four sub-time periods and the dark-grey circles based on the most balanced solution based on Scenario 1. The orange boxes in panel **(c)** indicate the deviations $\Delta I_{E,mt,O'} = I_{E,mt} - I_{E,O'}$ (Δ iii) based on all the Pareto front solutions for the four sub-time periods and the orange circles based on the most balanced solution for Scenario 2. The grey dots indicate the deviation $\Delta I_{E,O,O'}$ (Δ ii) between the observed $I_{E,O}$ for each sub-time period and the corresponding expected $I_{E,O'}$. The light-grey boxes in panel **(d)** indicate the deviations $\Delta I_{E,mT,O} = I_{E,mT} - I_{E,O}$ (Δ j) based on all the Pareto front solutions for the four sub-time periods and the grey circles based on the most balanced solution. The green boxes in panel **(d)** indicate the deviations $\Delta I_{E,mt,O} = I_{E,mt} - I_{E,O}$ (Δ jj) based on all the Pareto front solutions for the four sub-time periods and the green circles based on the most balanced solution.

from the observed I_E obtained from the time-invariant Scenario 1 are in most time periods, albeit only slightly, less pronounced (Fig. 11d).

5.5 Effect of S_{umax} on streamflow

Corresponding to the above findings, there is no significant difference in the modelled average streamflow between Scenario 1, using the long-term average S_{umax}, and Scenario 2, using individual S_{umax} values for each time period (Fig. 12d). While the model for both scenarios consistently and similarly underestimates high flows (Q^{5th}, Fig. 12a) by $\sim 10\,\%$, it overestimates median flows by $\sim 15\,\%$ with both time-invariant and time-variable S_{umax} for all time periods (Fig. 12b). Interestingly, the low flows are overpredicted by $\sim 10\,\%$–$20\,\%$ in the first two periods, while they are underpredicted by up to $\sim 20\,\%$ in the later periods in both scenarios (Fig. 12c). In addition, it was also found that using a time-variable S_{umax} in Scenario 2 did not have any discernible effect on the seasonal flow pattern (not shown). The fact that both scenarios generate similar estimates over different flow percentiles and, in particular, that the time-variable Scenario 2 reflects the same systematic shift in the ability of the model to reproduce low flows as Scenario 1 suggests, together with the very minor effects of the time-variable S_{umax} in Scenario 2 on the model performance metrics, that the adaptation of S_{umax} to changing climatic conditions does not significantly affect the average hydrological response pattern in the Neckar River basin.

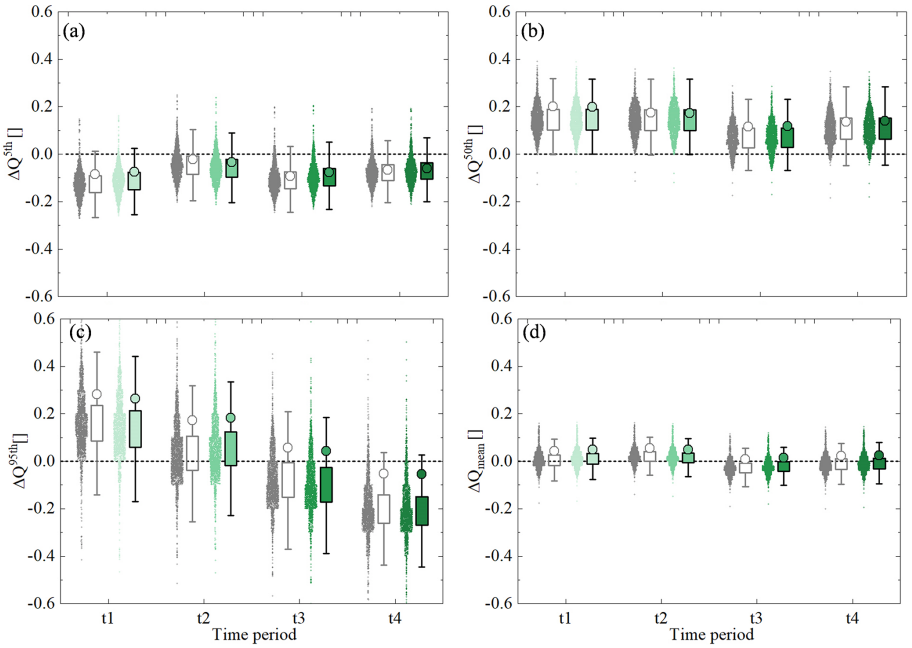

Figure 12. The relative errors of observed and modelled high ($Q^{5\text{th}}$), median ($Q^{50\text{th}}$), and low ($Q^{95\text{th}}$) flow quantiles and the mean Q for different time periods based on two scenarios. The grey shades and the corresponding dots indicate the relative errors based on Scenario 1 with all the Pareto front solutions, and the grey circles indicate the most balanced solution. The corresponding values for Scenario 2 are shown in green.

6 Discussion

6.1 Multi-decadal changes in root zone storage capacity S_{umax}

As Gao et al. (2024) suggested, considering the terrestrial ecosystem structure can improve our understanding of hydrological processes and how the ecosystem can survive and be developed. It is valuable to explore how ecosystems adapt to climatic variability (which is reflected in fluctuations in S_{umax}) and how this affects the long-term partitioning of drainage, evaporation, and hydrological response. This study is the first to systematically and explicitly quantify how the root zone storage capacity S_{umax} changes with changing climatic conditions over time. The values of root zone storage capacity, estimated from both water balance data and as a model calibration parameter, indeed show significant and corresponding fluctuations over multiple decades, varying by up to ±20 %. At $S_{\text{umax}} \sim 95$–115 mm, the overall estimated magnitudes fall well within the range of long-term average values reported previously for the greater region (e.g. Bouaziz et al., 2021; Hrachowitz et al., 2021; Tempel et al., 2024) and other temperate, humid environments (e.g. Kleidon, 2004; Gao et al., 2014b; de Boer et al., 2016; Wang-Erlandsson et al., 2016; Stocker et al., 2023; van Oorschot et al., 2024).

The values of S_{umax} obtained from both methods are very similar and within an error margin of only ∼5 %. In addition, they both follow a comparable change over time. Together, this lends support to the underlying assumption that this temporal evolution of S_{umax} may indeed be a fingerprint of vegetation adaptation to changing climatic conditions. More specifically, as $S_{\text{umax,WB}}$ is explicitly based on the estimates of transpiration E_{r} (Eq. 9), it could be plausibly argued that during specific years only more water is *used* for E_{r} but that the size of the water storage volume accessible for roots may not necessarily change. In that case, changes in $S_{\text{umax,WB}}$ would not reflect actual changes in the active root system but only in how much water was used by them. In contrast, $S_{\text{umax,cal}}$ inferred as a calibration parameter of a hydrological model regulates not only transpiration, but, critically, *also* the generation of streamflow. If therefore the active root system in reality did not change and fluctuations in $S_{\text{umax,WB}}$ were a mere artifact of changes in water uptake from a fixed-size volume instead of an actual change in maximum vegetation-accessible sub-surface water volumes, fluctuations in $S_{\text{umax,cal}}$ would not mirror those of $S_{\text{umax,WB}}$, and the use of $S_{\text{umax,WB}}$ in the hydrological model would, due to the non-linear character of the flow generation function in the model (Eq. S20 in Table S1), lead to misrepresentations of streamflow dynamics. However, no deteriorations of the model performance with a changing S_{umax} were found here. Even more, the fact that $S_{\text{umax,WB}}$ and $S_{\text{umax,cal}}$ are characterized by very similar magnitudes and fluctuations adds further evidence that their evolution over time is a manifestation

of vegetation adapting its active root system to changing climatic conditions.

Several previous studies in similar environments found that the root zone storage capacity S_{umax} can decrease by 50 % or more after deforestation and that these changes not only cause reductions in I_E by −0.2 or more, which reflect changes in ω and thus the overall functioning of the system, but also influence hydrological dynamics on short timescales, such as the magnitudes of flow peaks (Nijzink et al., 2016a; Hrachowitz et al., 2021). In contrast to the above studies, the ±20 % fluctuations of S_{umax} here did not lead to similarly marked shifts in I_E or ω. This is further corroborated by an analysis of different variables as potential controls on S_{umax} and ΔI_E as shown in Fig. 13. Fluctuations of S_{umax} can to a large extent be attributed to the variability in the ratio of winter precipitation to summer precipitation (Fig. 13s) as a simplified metric for precipitation seasonality. This comes as no surprise, as the computation of $S_{umax,WB}$ is explicitly based on the seasonal water deficit (Eq. 7). It merely shows that, when more precipitation falls in summer, at a time when evaporative demand is highest, the lower S_{umax} needs to provide vegetation with sufficient and continuous access to water for continuous vegetation transpiration. All the other tested variables do not exert any major influence on S_{umax} in the study region. Conversely, it was found that the deviations ΔI_E are largely independent of the seasonality of precipitation (Fig. 13g). Instead, increases in summer E_P are correlated with decreases in ΔI_E (Fig. 13h) and thus with a reduction in E_T. The observed systematic shift towards a more negative ΔI_E, which indicates proportionally less evaporation, thus coincides with the gradually increasing summer E_P over time. This points towards different controls on ΔI_E than on S_{umax} and the potential role of increased vegetation water stress in summer as the main driver of ΔI_E. Thus, while there is compelling evidence of fluctuations in S_{umax}, the above illustrates that these changes cannot explain the observed deviations from the expected long-term Budyko trajectory in the study region.

It is also important to note that the temporal fluctuations of both S_{umax} and ΔI_E can be subject to uncertainties. In spite of the findings reported by Han et al. (2020) that, for most river catchments worldwide, $dS/dt \sim 0$ holds over averaging periods similar to the ones used here (t_1–t_4), this assumption may not completely hold in the study region. In relation to this, we did not consider potential effects of unobserved groundwater import or export on the long-term water balance either (Bouaziz et al., 2018).

As only < 2 % of the study area experienced documented land use change over the 1953–2022 period and no major reservoirs are present upstream of the study basin outlet, here we interpret fluctuations in S_{umax} as being a reflection of adaptations of root systems to changing hydro-climatic conditions. However, some of the fluctuations may be a consequence of land management practices not quantified by available gridded land cover products such as CORINE, including forest thinning (Hrachowitz et al., 2021) or rejuvenation (Teuling and Hoek van Dijke, 2020). In addition, although here we mainly attribute changes in S_{umax} to changes in root systems, these may be complemented by additional effects of changes in vegetation water use due to feedbacks with increases in atmospheric CO_2 (e.g. Berghuijs et al., 2017; Jaramillo et al., 2018).

6.2 Effect of changing S_{umax} on the representation of streamflow in a model

Reflecting their lack of explanatory power for the changes in ΔI_E, our results correspondingly indicate that signatures of both annual flow, such as the average Q^{5th}, Q^{50th}, or Q^{95th}, and seasonal flow are not reproduced better by the hydrological model when replacing a time-invariant, long-term average S_{umax} with a temporally dynamic S_{umax}. Overall, these results are in contrast to previous studies that quantified the effect of a time-variable S_{umax} parameter following deforestation. For example, Nijzink et al. (2016a) reported that adjusting the parameter S_{umax} to a lower value improves a model's ability to reproduce streamflow after deforestation. These findings were strongly supported by Hrachowitz et al. (2021), who found that post-deforestation model recalibration resulted in a lower S_{umax} and a significantly better performance compared to using parameters from pre-deforestation calibration. However, our results are also different from those reported by Duethmann et al. (2020), who found that accounting for vegetation dynamics in a model in the form of changing surface resistances to vegetation improved the long-term performance of the model. Similarly, Bouaziz et al. (2022) estimated the future S_{umax} based on projected future hydro-climatic conditions. In a somewhat more humid environment, they found that an estimated ∼ 25 % future increase in S_{umax} from ∼ 170 to 226 mm may lead to reductions in the mean and maximum annual Q of ∼ 5 %. More pronounced effects were reported on the intra-annual timescale, with reductions in autumn and winter Q of up to ∼ 15 %. This was accompanied by increases of up to ∼ 15 % in summer evaporation and decreases of 10 % in winter groundwater levels. Irrespective of the additional uncertainties in their study introduced by future projections, the much less pronounced effects we found in our analysis are most likely a consequence of the lower absolute magnitude of S_{umax} that remains below 115 mm in the study region. These lower S_{umax} values reflect lower storage requirements in summer, due to a precipitation pattern in the Neckar River basin that is more evenly spread throughout the year. In other words, the fact that here ∼ 55 %–60 % of the annual precipitation falls in summer (Fig. 3f and k) when it is needed most by vegetation due to high E_P removes the need for a larger S_{umax} as a water storage buffer to allow vegetation to survive. However, the lower the magnitude of S_{umax}, the more frequently storage deficits can be overcome by even rather small rainstorms and the less water is (or needs to be) stored. Thus,

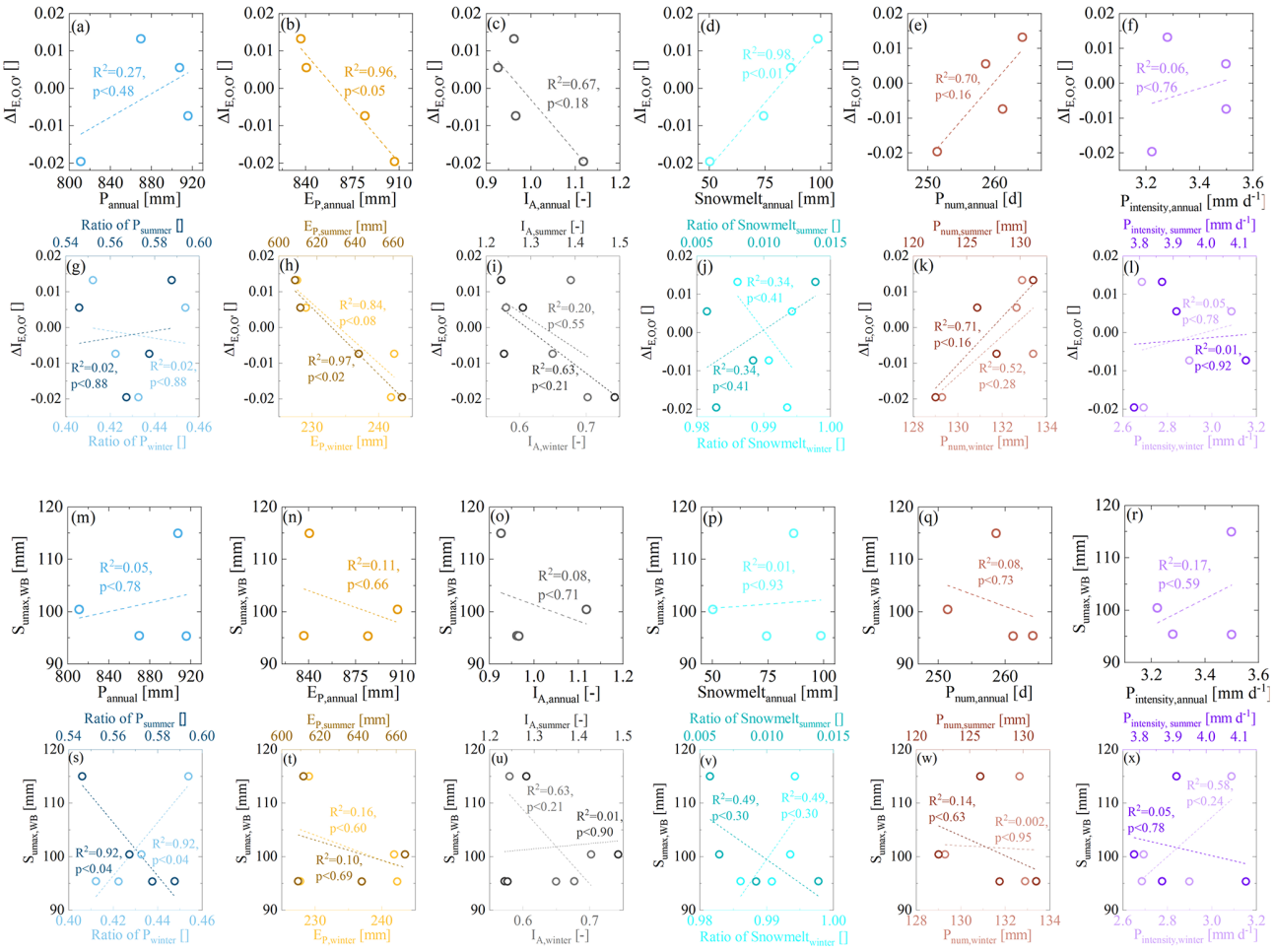

Figure 13. Relationships between the temporal fluctuation of the deviations ($\Delta I_{E,O,O'}$, black dots in Fig. 10a), $S_{umax,WB}$, and climate indices, including precipitation (P), potential evaporation (E_P), the aridity index (I_A), the estimated snowmelt water (Snowmelt), the number of precipitation days (P_{num}), and the precipitation intensity ($P_{intensity}$) for the four sub-time periods. Relationships between the temporal fluctuation of the deviations ($\Delta I_{E,O,O'}$, black dots in Fig. 10a) and the climate indices for the four sub-time periods are shown in the first two rows in panels **(a–l)** (i.e. **(a–f)** $\Delta I_{E,O,O'}$ vs. annual climatic indices and **(g–l)** $\Delta I_{E,O,O'}$ vs. seasonal climatic indices). Relationships between the temporal fluctuation of $S_{umax,WB}$ derived from the water balance method and climate indices for the four sub-time periods are shown in the last two rows in panels **(m–x)** (i.e. **(m–r)** $S_{umax,WB}$ vs. annual climatic indices and **(s–x)** $S_{umax,WB}$ vs. seasonal climatic indices).

even if the relative changes are similar between Bouaziz et al. (2022) and Tempel et al. (2024) in a somewhat more humid environment and our study, abundant summer precipitation causes absolute S_{umax} fluctuations of less than ± 20 mm over time in the Neckar catchment. This in turn limits the influence of the changes on the hydrological response, which has wider implications for the use of models in the Neckar River basin and potentially in other temperate regions with similar hydro-climatic characteristics. More specifically, it has been argued that a changing climate will affect the properties of terrestrial hydrological systems (e.g. Stevens et al., 2020). As these properties are represented by typically time-invariant parameters in hydrological or land surface models, accounting for changing system properties with time-variable formulations of parameters may facilitate more reliable predictions. For many model parameters such a time-variable formulation to estimate their future values is not trivial due to frequently insufficient data and a general lack of mechanistic understanding of the underlying processes. The estimation of S_{umax} and its temporal evolution based on observed historical or projected future water balance data opens up an opportunity to estimate its magnitude under future conditions for use in models. However, in contrast to the findings in other regions (e.g. Merz et al., 2011) and as discussed above, adapting S_{umax} to changing conditions in the Neckar River basin does not lead to improved modelled representations of the hydrological response. It is therefore plausible to assume that the use of a time-variable parameter S_{umax} does not substantially improve future predictions and is thus not necessarily required for at least the next few decades to

come and that the use of a long-term average S_{umax}, obtained either by calibration or based on the water balance, is sufficient in the Neckar River basin and in hydro-climatically similar regions. This in itself is already an interesting finding as it gives modellers process-based evidence that the use of a time-invariant S_{umax} as a model parameter will also be sufficient for meaningful hydrological predictions in the near future in such an environment. However, it can also be expected that, in more arid regions with less summer precipitation and generally higher S_{umax} (see e.g. Gao et al., 2014b; Stocker et al., 2023), changes in S_{umax} will play a more prominent role.

7 Conclusions

The catchment-scale root zone storage capacity (S_{umax}) is a critical factor reflecting the moisture exchange between land and atmosphere as well as the hydrological response in terrestrial hydrological systems. However, as a major knowledge gap, it is unclear whether S_{umax} at the catchment scale evolves over time, reflecting vegetation adaptation to changing climatic conditions. As a consequence, it also remains unclear how potential changes in S_{umax} may affect the partitioning of water fluxes and, as a consequence, the catchment-scale hydrological response. In this study, for the upper Neckar catchment, based on long-term daily hydrological data (1953–2022), we quantify and analyse how S_{umax} dynamically evolves over multiple decades, reflecting vegetation adaptation to climate variability and the effects on the hydrological system.

The main findings of our analysis are the following:

1. S_{umax} has fluctuated by $\pm 20\,\%$ between 95 and 115 mm, in response to climatic variability over the 70-year study period.

2. Estimates of S_{umax} obtained from both methods, i.e. based on water balance data and model calibration parameters, respectively, were, with differences of $\sim 5\,\%$, highly consistent with each other and correlated in time ($R^2 = 0.95$, $p = 0.05$). Findings (1) and (2) support the hypothesis that S_{umax}, even in temperate, humid climates such as in the Neckar River basin, significantly changes over multiple decades, reflecting vegetation adaptation to climatic variability.

3. The estimated fluctuations of S_{umax} were inconsistent with the temporal sequence of observed deviations $\Delta I_E \sim \pm 0.02$ from the expected I_E over the study period ($R^2 = 0.02$, $p = 0.85$).

4. As a consequence, replacing a long-term average, time-invariant parameter S_{umax} in a hydrological model with a time-variable formulation of S_{umax} does not lead to a better representation of the observed ΔI_E. Based on (3) and (4), the hypothesis that S_{umax} affects the long-term partitioning of drainage and evaporation and thus controls deviations ΔI_E from the catchment-specific trajectory in the Budyko space needs to be rejected for the Neckar River basin.

5. Replacing the time-invariant S_{umax} with a time-variable S_{umax} in the hydrological model leads to only very minor improvements of the model to reproduce streamflow dynamics. The hypothesis that a time-dynamic implementation of S_{umax} improves the representation of streamflow in the hydrological model therefore also needs to be rejected for the Neckar River basin.

Overall, our study is the first to systematically document the temporal evolution of S_{umax}, and although limited to the Neckar River basin, it provides clear quantitative evidence that S_{umax} can significantly change over multiple decades, reflecting vegetation adaptation to climate variability. However, these changes do not cause deviations from the long-term average Budyko curve under changing climatic conditions. This implies that the temporal evolution of S_{umax} does not control variation in the partitioning of water fluxes and has no significant effects on fundamental hydrological response characteristics of the upper Neckar River basin. As the use of time-variable S_{umax} over the 70-year study period does not improve the performance of the hydrological model, it can plausibly be assumed that in the study region the use of time-invariant S_{umax} as a model parameter will be sufficient for meaningful predictions over at least the next few decades.

Code and data availability. The model codes underlying this paper are available online in the 4TU data repository (DOI: https://doi.org/10.4121/922d30de-a26b-4c81-8644-ad036182239c, Wang and Hrachowitz, 2024). The equations used in the model are described in the Supplement The meteorological and hydrological data used in this study can be obtained from the German Weather Service (DWD) (https://opendata.dwd.de/climate_environment/CDC/observations_germany/climate/daily/more_precip/historical/, DWD, 2024) and the German Federal Institute of Hydrology (BfG) (https://portal.grdc.bafg.de/applications/public.html?publicuser=PublicUser#dataDownload/Stations, BfG, 2024).

Supplement. The supplement related to this article is available online at: https://doi.org/10.5194/hess-28-4011-2024-supplement.

Author contributions. SW, MH, and GS designed the study. SW performed the experiments. All the authors contributed to the general idea, the discussion, and the writing of the manuscript.

Competing interests. At least one of the (co-)authors is a member of the editorial board of *Hydrology and Earth System Sciences*. The peer-review process was guided by an independent editor, and the authors also have no other competing interests to declare.

Acknowledgements. We gratefully acknowledge the financial support from the China Scholarship Council (CSC).

Financial support. This research has been supported by the Chinese Research Council (grant no. 202006190030).

Review statement. This paper was edited by Fuqiang Tian and reviewed by Lele Shu and two anonymous referees.

References

AghaKouchak, A., Feldman, D., Hoerling, M., Huxman, T., and Lund, J.: Water and climate: Recognize anthropogenic drought, Nature, 524, 409–411, https://doi.org/10.1038/524409a, 2015.

Ajami, N. K., Gupta, H., Wagener, T., and Sorooshian, S.: Calibration of a semi-distributed hydrologic model for streamflow estimation along a river system, J. Hydrol., 298, 112–135, https://doi.org/10.1016/j.jhydrol.2004.03.033, 2004.

Alila, Y., Kuraś, P. K., Schnorbus, M., and Hudson, R.: Forests and floods: A new paradigm sheds light on age-old controversies, Water Resour. Res., 45, W08416, https://doi.org/10.1029/2008WR007207, 2009.

Bahremand, A. and Hosseinalizadeh, M.: Development of conceptual hydrological FLEX-Topo model for loess watersheds influenced by piping and tunnel erosion in Golestan Province of Iran, Journal of Water and Soil Conservation, 29, 115–133, https://doi.org/10.22069/jwsc.2022.20050.3544, 2022.

Berghuijs, W. R. and Woods, R.: A simple framework to quantitatively describe monthly precipitation and temperature climatology, Int. J. Climatol., 36, 3161–3174, https://doi.org/10.1002/joc.4544, 2016.

Berghuijs, W. R., Larsen, J. R., Van Emmerik, T. H., and Woods, R. A.: A global assessment of runoff sensitivity to changes in precipitation, potential evaporation, and other factors, Water Resour. Res., 53, 8475–8486, https://doi.org/10.1002/2017WR021593, 2017.

BfG: Streamflow datasets in Germany, BfG [data set], https://portal.grdc.bafg.de/applications/public.html?publicuser=PublicUser#dataDownload/Stations, last access: 27 August 2024.

Bouaziz, L., Weerts, A., Schellekens, J., Sprokkereef, E., Stam, J., Savenije, H., and Hrachowitz, M.: Redressing the balance: quantifying net intercatchment groundwater flows, Hydrol. Earth Syst. Sci., 22, 6415–6434, https://doi.org/10.5194/hess-22-6415-2018, 2018.

Bouaziz, L. J., Steele-Dunne, S. C., Schellekens, J., Weerts, A. H., Stam, J., Sprokkereef, E., Winsemius, H. H., Savenije, H. H., and Hrachowitz, M.: Improved understanding of the link between catchment-scale vegetation accessible storage and satellite-derived Soil Water Index, Water Resour. Res., 56, e2019WR026365, https://doi.org/10.1029/2019WR026365, 2020.

Bouaziz, L. J. E., Fenicia, F., Thirel, G., de Boer-Euser, T., Buitink, J., Brauer, C. C., De Niel, J., Dewals, B. J., Drogue, G., Grelier, B., Melsen, L. A., Moustakas, S., Nossent, J., Pereira, F., Sprokkereef, E., Stam, J., Weerts, A. H., Willems, P., Savenije, H. H. G., and Hrachowitz, M.: Behind the scenes of streamflow model performance, Hydrol. Earth Syst. Sci., 25, 1069–1095, https://doi.org/10.5194/hess-25-1069-2021, 2021.

Bouaziz, L. J. E., Aalbers, E. E., Weerts, A. H., Hegnauer, M., Buiteveld, H., Lammersen, R., Stam, J., Sprokkereef, E., Savenije, H. H. G., and Hrachowitz, M.: Ecosystem adaptation to climate change: the sensitivity of hydrological predictions to time-dynamic model parameters, Hydrol. Earth Syst. Sci., 26, 1295–1318, https://doi.org/10.5194/hess-26-1295-2022, 2022.

Brath, A., Montanari, A., and Moretti, G.: Assessing the effect on flood frequency of land use change via hydrological simulation (with uncertainty), J. Hydrol., 324, 141–153, https://doi.org/10.1016/j.jhydrol.2005.10.001, 2006.

Brown, D. G., Johnson, K. M., Loveland, T. R., and Theobald, D. M.: Rural land-use trends in the conterminous United States, 1950–2000, Ecol. Appl., 15, 1851–1863, https://doi.org/10.1890/03-5220, 2005.

Budyko, M. I.: Climate and Life, Academic Press, New York, 508 pp., ISBN 9780080954530, 1974.

Coenders-Gerrits, A. M. J., Van der Ent, R. J., Bogaard, T. A., Wang-Erlandsson, L., Hrachowitz, M., and Savenije, H. H. G.: Uncertainties in transpiration estimates, Nature, 506, E1–E2, https://doi.org/10.1038/nature12925, 2014.

de Boer-Euser, T., McMillan, H. K., Hrachowitz, M., Winsemius, H. C., and Savenije, H. H.: Influence of soil and climate on root zone storage capacity, Water Resour. Res., 52, 2009–2024, https://doi.org/10.1002/2015WR018115, 2016.

Donohue, R. J., Roderick, M. L., and McVicar, T. R.: On the importance of including vegetation dynamics in Budyko's hydrological model, Hydrol. Earth Syst. Sci., 11, 983–995, https://doi.org/10.5194/hess-11-983-2007, 2007.

Donohue, R. J., Roderick, M. L., and McVicar, T. R.: Roots, storms and soil pores: Incorporating key ecohydrological processes into Budyko's hydrological model, J. Hydrol., 436, 35–50, https://doi.org/10.1016/j.jhydrol.2012.02.033, 2012.

Dralle, D. N., Hahm, W. J., Chadwick, K. D., McCormick, E., and Rempe, D. M.: Technical note: Accounting for snow in the estimation of root zone water storage capacity from precipitation and evapotranspiration fluxes, Hydrol. Earth Syst. Sci., 25, 2861–2867, https://doi.org/10.5194/hess-25-2861-2021, 2021.

Duethmann, D., Blöschl, G., and Parajka, J.: Why does a conceptual hydrological model fail to correctly predict discharge changes in response to climate change?, Hydrol. Earth Syst. Sci., 24, 3493–3511, https://doi.org/10.5194/hess-24-3493-2020, 2020.

DWD: Index of /climate_environment/CDC/observations_germany/climate/daily/more_precip/historical/, DWD [data set], https://opendata.dwd.de/climate_environment/CDC/observations_germany/climate/daily/more_precip/historical/, last access: 27 August 2024.

Efstratiadis, A. and Koutsoyiannis, D.: One decade of multi-objective calibration approaches in hydrologi-

cal modelling: a review, Hydrolog. Sci. J., 55, 58–78, https://doi.org/10.1080/02626660903526292, 2010.

Ellison, D., Pokorný, J., and Wild, M.: Even cooler insights: On the power of forests to (water the Earth and) cool the planet, Glob. Change Biol., 30, e17195, https://doi.org/10.1111/gcb.17195, 2024.

Euser, T., Hrachowitz, M., Winsemius, H. C., and Savenije, H. H.: The effect of forcing and landscape distribution on performance and consistency of model structures, Hydrol. Process., 29, 3727–3743, https://doi.org/10.1002/hyp.10445, 2015.

Fan, Y., Miguez-Macho, G., Jobbágy, E. G., Jackson, R. B., and Otero-Casal, C.: Hydrologic regulation of plant rooting depth, P. Natl. Acad. Sci. USA, 114, 10572–10577, https://doi.org/10.1073/pnas.1712381114, 2017.

Fenicia, F., Savenije, H. H., Matgen, P., and Pfister, L.: Understanding catchment behavior through stepwise model concept improvement, Water Resour. Res., 44, W01402, https://doi.org/10.1029/2006WR005563, 2008.

Fenicia, F., Savenije, H. H. G., and Avdeeva, Y.: Anomaly in the rainfall-runoff behaviour of the Meuse catchment, Climate, land-use, or land-use management?, Hydrol. Earth Syst. Sci., 13, 1727–1737, https://doi.org/10.5194/hess-13-1727-2009, 2009.

Fu, B.: On the calculation of the evaporation from land surface, Scientia Atmospherica Sinica, 5, 23–31, 1981 (in Chinese).

Gao, H., Hrachowitz, M., Fenicia, F., Gharari, S., and Savenije, H. H. G.: Testing the realism of a topography-driven model (FLEX-Topo) in the nested catchments of the Upper Heihe, China, Hydrol. Earth Syst. Sci., 18, 1895–1915, https://doi.org/10.5194/hess-18-1895-2014, 2014a.

Gao, H., Hrachowitz, M., Schymanski, S., Fenicia, F., Sriwongsitanon, N., and Savenije, H.: Climate controls how ecosystems size the root zone storage capacity at catchment scale, Geophys. Res. Lett., 41, 7916–7923, https://doi.org/10.1002/2014GL061668, 2014b.

Gao, H., Hrachowitz, M., Wang-Erlandsson, L., Fenicia, F., Xi, Q., Xia, J., Shao, W., Sun, G., and Savenije, H.: Root zone in the Earth system, EGUsphere [preprint], https://doi.org/10.5194/egusphere-2024-332, 2024.

Gentine, P., D'Odorico, P., Lintner, B. R., Sivandran, G., and Salvucci, G.: Interdependence of climate, soil, and vegetation as constrained by the Budyko curve, Geophys. Res. Lett., 39, L19404, https://doi.org/10.1029/2012GL053492, 2012.

Gharari, S., Hrachowitz, M., Fenicia, F., and Savenije, H. H. G.: Hydrological landscape classification: investigating the performance of HAND based landscape classifications in a central European meso-scale catchment, Hydrol. Earth Syst. Sci., 15, 3275–3291, https://doi.org/10.5194/hess-15-3275-2011, 2011.

Gharari, S., Hrachowitz, M., Fenicia, F., and Savenije, H. H. G.: An approach to identify time consistent model parameters: sub-period calibration, Hydrol. Earth Syst. Sci., 17, 149–161, https://doi.org/10.5194/hess-17-149-2013, 2013.

Gharari, S., Hrachowitz, M., Fenicia, F., Gao, H., and Savenije, H. H. G.: Using expert knowledge to increase realism in environmental system models can dramatically reduce the need for calibration, Hydrol. Earth Syst. Sci., 18, 4839–4859, https://doi.org/10.5194/hess-18-4839-2014, 2014.

Goovaerts, P.: Geostatistical approaches for incorporating elevation into the spatial interpolation of rainfall, J. Hydrol., 228, 113–129, https://doi.org/10.1016/S0022-1694(00)00144-X, 2000.

Gumbel, E. J.: The return period of flood flows, Ann. Math. Stat., 12, 163–190, https://doi.org/10.1214/aoms/1177731747, 1941.

Guswa, A. J.: The influence of climate on root depth: A carbon cost-benefit analysis, Water Resour. Res., 44, W02427, https://doi.org/10.1029/2007WR006384, 2008.

Hadka, D. and Reed, P.: Borg: An auto-adaptive many-objective evolutionary computing framework, Evolutionary Computation, 21, 231–259, https://doi.org/10.1029/2007WR006384, 2013.

Han, J., Yang, Y., Roderick, M. L., McVicar, T. R., Yang, D., Zhang, S., and Beck, H. E. , Assessing the steady-state assumption in water balance calculation across global catchments, Water Resour. Res., 56, e2020WR027392, https://doi.org/10.1029/2020WR027392, 2020.

Hanus, S., Hrachowitz, M., Zekollari, H., Schoups, G., Vizcaino, M., and Kaitna, R.: Future changes in annual, seasonal and monthly runoff signatures in contrasting Alpine catchments in Austria, Hydrol. Earth Syst. Sci., 25, 3429–3453, https://doi.org/10.5194/hess-25-3429-2021, 2021.

Hoek van Dijke, A. J., Herold, M., Mallick, K., Benedict, I., Machwitz, M., Schlerf, M., Pranindita, A., Theeuwen, J. J., Bastin, J.-F., and Teuling, A. J.: Shifts in regional water availability due to global tree restoration, Nat. Geosci., 15, 363–368, https://doi.org/10.1038/s41561-022-00935-0, 2022.

Hrachowitz, M. and Weiler, M.: Uncertainty of precipitation estimates caused by sparse gauging networks in a small, mountainous watershed, J. Hydrol. Eng., 16, 460–471, https://doi.org/10.1061/(ASCE)HE.1943-5584.0000331, 2011.

Hrachowitz, M., Fovet, O., Ruiz, L., Euser, T., Gharari, S., Nijzink, R., Freer, J., Savenije, H., and Gascuel-Odoux, C.: Process consistency in models: The importance of system signatures, expert knowledge, and process complexity, Water Resour. Res., 50, 7445–7469, https://doi.org/10.1002/2014WR015484, 2014.

Hrachowitz, M., Stockinger, M., Coenders-Gerrits, M., van der Ent, R., Bogena, H., Lücke, A., and Stumpp, C.: Reduction of vegetation-accessible water storage capacity after deforestation affects catchment travel time distributions and increases young water fractions in a headwater catchment, Hydrol. Earth Syst. Sci., 25, 4887–4915, https://doi.org/10.5194/hess-25-4887-2021, 2021.

Hulsman, P., Hrachowitz, M., and Savenije, H. H.: Improving the representation of long-term storage variations with conceptual hydrological models in data-scarce regions, Water Resour. Res., 57, e2020WR028837, https://doi.org/10.1029/2020WR028837, 2021a.

Hulsman, P., Savenije, H. H. G., and Hrachowitz, M.: Learning from satellite observations: increased understanding of catchment processes through stepwise model improvement, Hydrol. Earth Syst. Sci., 25, 957–982, https://doi.org/10.5194/hess-25-957-2021, 2021b.

Ibrahim, M., Coenders-Gerrits, M., van der Ent, R., and Hrachowitz, M.: Catchments do not strictly follow Budyko curves over multiple decades but deviations are minor and predictable, Hydrol. Earth Syst. Sci. Discuss. [preprint], https://doi.org/10.5194/hess-2024-120, in review, 2024.

Jaramillo, F. and Destouni, G.: Developing water change spectra and distinguishing change drivers worldwide, Geophys. Res. Lett., 41, 8377–8386, https://doi.org/10.1002/2014GL061848, 2014.

Jaramillo, F., Cory, N., Arheimer, B., Laudon, H., van der Velde, Y., Hasper, T. B., Teutschbein, C., and Uddling, J.: Dominant effect of increasing forest biomass on evapotranspiration: interpretations of movement in Budyko space, Hydrol. Earth Syst. Sci., 22, 567–580, https://doi.org/10.5194/hess-22-567-2018, 2018.

Jasechko, S.: Plants turn on the tap, Nat. Clim. Change, 8, 562–563, https://doi.org/10.1038/s41558-018-0212-z, 2018.

Kleidon, A.: Beyond Gaia: Thermodynamics of Life and Earth System Functioning, Climatic Change, 66, 271–319, https://doi.org/10.1023/B:CLIM.0000044616.34867.ec, 2004.

Laio, F., Porporato, A., Ridolfi, L., and Rodriguez-Iturbe, I.: Plants in water-controlled ecosystems: active role in hydrologic processes and response to water stress: II. Probabilistic soil moisture dynamics, Adv. Water Resour., 24, 707–723, https://doi.org/10.1016/S0309-1708(01)00005-7, 2001.

Liancourt, P., Sharkhuu, A., Ariuntsetseg, L., Boldgiv, B., Helliker, B. R., Plante, A. F., Petraitis, P. S., and Casper, B. B.: Temporal and spatial variation in how vegetation alters the soil moisture response to climate manipulation, Plant Soil, 351, 249–261, https://doi.org/10.1007/s11104-011-0956-y, 2012.

Lloyd, C.: Assessing the effect of integrating elevation data into the estimation of monthly precipitation in Great Britain, J. Hydrol., 308, 128–150, https://doi.org/10.1016/j.jhydrol.2004.10.026, 2005.

McCormick, E. L., Dralle, D. N., Hahm, W. J., Tune, A. K., Schmidt, L. M., Chadwick, K. D., and Rempe, D. M.: Widespread woody plant use of water stored in bedrock, Nature, 597, 225–229, https://doi.org/10.1038/s41586-021-03761-3, 2021.

McMurtrie, R. E., Iversen, C. M., Dewar, R. C., Medlyn, B. E., Näsholm, T., Pepper, D. A., and Norby, R. J.: Plant root distributions and nitrogen uptake predicted by a hypothesis of optimal root foraging, Ecol. Evol., 2, 1235–1250, https://doi.org/10.1002/ece3.266, 2012.

Merz, R., Parajka, J., and Blöschl, G.: Time stability of catchment model parameters: Implications for climate impact analyses, Water Resour. Res., 47, W02531, https://doi.org/10.1029/2010WR009505, 2011.

Mianabadi, A., Coenders-Gerrits, M., Shirazi, P., Ghahraman, B., and Alizadeh, A.: A global Budyko model to partition evaporation into interception and transpiration, Hydrol. Earth Syst. Sci., 23, 4983–5000, https://doi.org/10.5194/hess-23-4983-2019, 2019.

Miralles, D. G., Brutsaert, W., Dolman, A. J., and Gash, J. H.: On the use of the term "evapotranspiration", Water Resour. Res., 56, e2020WR028055, https://doi.org/10.1029/2020WR028055, 2020.

Nijzink, R., Hutton, C., Pechlivanidis, I., Capell, R., Arheimer, B., Freer, J., Han, D., Wagener, T., McGuire, K., Savenije, H., and Hrachowitz, M.: The evolution of root-zone moisture capacities after deforestation: a step towards hydrological predictions under change?, Hydrol. Earth Syst. Sci., 20, 4775–4799, https://doi.org/10.5194/hess-20-4775-2016, 2016a.

Nijzink, R. C., Samaniego, L., Mai, J., Kumar, R., Thober, S., Zink, M., Schäfer, D., Savenije, H. H. G., and Hrachowitz, M.: The importance of topography-controlled sub-grid process heterogeneity and semi-quantitative prior constraints in distributed hydrological models, Hydrol. Earth Syst. Sci., 20, 1151–1176, https://doi.org/10.5194/hess-20-1151-2016, 2016b.

Nijzink, R., Almeida, S., Pechlivanidis, I., Capell, R., Gustafssons, D., Arheimer, B., Parajka, J., Freer, J., Han, D., and Wagener, T.: Constraining conceptual hydrological models with multiple information sources, Water Resour. Res., 54, 8332–8362, https://doi.org/10.1029/2017WR021895, 2018.

Ol'Dekop, E.: On evaporation from the surface of river basins, Transactions on Meteorological Observations, 4, 200, https://scholar.google.com/scholar_lookup?hl=en&volume=4&publication_year=1911&pages=200&journal=Trans.+Meteorol.+Obs.+Univ.+Tartu&author=E.+M.+Ol%27dekop&title=On+evaporation+from+the+surface+of+river+basins (last access: 27 August 2024), 1911.

Oudin, L., Hervieu, F., Michel, C., Perrin, C., Andréassian, V., Anctil, F., and Loumagne, C.: Which potential evapotranspiration input for a lumped rainfall–runoff model?: Part 2—Towards a simple and efficient potential evapotranspiration model for rainfall–runoff modelling, J. Hydrol., 303, 290–306, https://doi.org/10.1016/j.jhydrol.2004.08.026, 2005.

Oudin, L., Andréassian, V., Lerat, J., and Michel, C.: Has land cover a significant impact on mean annual streamflow? An international assessment using 1508 catchments, J. Hydrol., 357, 303–316, https://doi.org/10.1016/j.jhydrol.2008.05.021, 2008.

Prenner, D., Kaitna, R., Mostbauer, K., and Hrachowitz, M.: The value of using multiple hydrometeorological variables to predict temporal debris flow susceptibility in an alpine environment, Water Resour. Res., 54, 6822–6843, https://doi.org/10.1029/2018WR022985, 2018.

Reaver, N. G. F., Kaplan, D. A., Klammler, H., and Jawitz, J. W.: Theoretical and empirical evidence against the Budyko catchment trajectory conjecture, Hydrol. Earth Syst. Sci., 26, 1507–1525, https://doi.org/10.5194/hess-26-1507-2022, 2022.

Roberts, K. J., Dietrich, J. C., Wirasaet, D., Pringle, W. J., and Westerink, J. J.: Dynamic load balancing for predictions of storm surge and coastal flooding, Environ. Modell. Softw., 140, 105045, https://doi.org/10.1016/j.envsoft.2021.105045, 2021.

Roderick, M. L. and Farquhar, G. D.: A simple framework for relating variations in runoff to variations in climatic conditions and catchment properties, Water Resour. Res., 47, W00G07, https://doi.org/10.1029/2010WR009826, 2011.

Rodríguez-Iturbe, I. and Porporato, A.: Ecohydrology of water-controlled ecosystems: soil moisture and plant dynamics, Cambridge University Press, ISBN 9780521036740, https://www.cambridge.org/us/universitypress/subjects/earth-and-environmental-science/hydrology-hydrogeology-and-water-resources/ecohydrology-water-controlled-ecosystems-soil-moisture-and-plant-dynamics?format=PB&isbn=9780521036740 (last access: 27 August 2024), 2007.

Roodari, A., Hrachowitz, M., Hassanpour, F., and Yaghoobzadeh, M.: Signatures of human intervention – or not? Downstream intensification of hydrological drought along a large Central Asian river: the individual roles of climate variability and land use change, Hydrol. Earth Syst. Sci., 25, 1943–1967, https://doi.org/10.5194/hess-25-1943-2021, 2021.

Sadayappan, K., Keen, R., Jarecke, K. M., Moreno, V., Nippert, J. B., Kirk, M. F., Sullivan, P. L., and Li, L.: Drier streams despite a wetter climate in woody-encroached grasslands, J. Hydrol., 627, 130388, https://doi.org/10.1016/j.jhydrol.2023.130388, 2023.

Savenije, H. H.: The importance of interception and why we should delete the term evapotranspiration from our vocabulary, Hydrol. Process., 18, 1507–1511, https://doi.org/10.1002/hyp.5563, 2004.

Savenije, H. H. G. and Hrachowitz, M.: HESS Opinions "Catchments as meta-organisms – a new blueprint for hydrological modelling", Hydrol. Earth Syst. Sci., 21, 1107–1116, https://doi.org/10.5194/hess-21-1107-2017, 2017.

Schenk, H. J. and Jackson, R. B.: Rooting depths, lateral root spreads and below-ground/above-ground allometries of plants in water-limited ecosystems, J. Ecol., 90, 480–494, https://www.jstor.org/stable/3072232 (last access: 24 August 2024), 2002.

Schreiber, P.: Über die Beziehungen zwischen dem Niederschlag und der Wasserführung der Flüsse in Mitteleuropa, Z. Meteorol., 21, 441–452, 1904.

Scrivner, C. and Ruppert, D.: Thickness of soil solum as a parameter of plant-available water storage capacity in soils underlain by carbonate rocks, University of Missouri-Columbia, https://hdl.handle.net/10355/91873 (last access: 24 August 2024), 1970.

Singh, C., Wang-Erlandsson, L., Fetzer, I., Rockström, J., and Van Der Ent, R.: Rootzone storage capacity reveals drought coping strategies along rainforest-savanna transitions, Environ. Res. Lett., 15, 124021, https://doi.org/10.1088/1748-9326/abc377, 2020.

Sivandran, G. and Bras, R. L.: Identifying the optimal spatially and temporally invariant root distribution for a semiarid environment, Water Resour. Res., 48, W12525, https://doi.org/10.1029/2012WR012055, 2012.

Sivandran, G. and Bras, R. L.: Dynamic root distributions in ecohydrological modeling: A case study at Walnut Gulch Experimental Watershed, Water Resour. Res., 49, 3292–3305, https://doi.org/10.1002/wrcr.20245, 2013.

Speich, M. J. R., Lischke, H., and Zappa, M.: Testing an optimality-based model of rooting zone water storage capacity in temperate forests, Hydrol. Earth Syst. Sci., 22, 4097–4124, https://doi.org/10.5194/hess-22-4097-2018, 2018.

Sriwongsitanon, N., Jandang, W., Williams, J., Suwawong, T., Maekan, E., and Savenije, H. H. G.: Using normalised difference infrared index patterns to constrain semi-distributed rainfall–runoff models in tropical nested catchments, Hydrol. Earth Syst. Sci., 27, 2149–2171, https://doi.org/10.5194/hess-27-2149-2023, 2023.

Stephens, C. M., Lall, U., Johnson, F., and Marshall, L. A.: Landscape changes and their hydrologic effects: Interactions and feedbacks across scales, Earth-Sci. Rev., 212, 103466, https://doi.org/10.1016/j.earscirev.2020.103466, 2021.

Stevens, J. T., Boisramé, G. F., Rakhmatulina, E., Thompson, S. E., Collins, B. M., and Stephens, S. L.: Forest vegetation change and its impacts on soil water following 47 years of managed wildfire, Ecosystems, 23, 1547–1565, https://doi.org/10.1007/s10021-020-00489-5, 2020.

Stocker, B. D., Tumber-Dávila, S. J., Konings, A. G., Anderson, M. C., Hain, C., and Jackson, R. B.: Global patterns of water storage in the rooting zones of vegetation, Nat. Geosci., 16, 250–256, https://doi.org/10.1038/s41561-023-01125-2, 2023.

Tempel, N. T., Bouaziz, L., Taormina, R., van Noppen, E., Stam, J., Sprokkereef, E., and Hrachowitz, M.: Vegetation Response to Climatic Variability: Implications for Root Zone Storage and Streamflow Predictions, EGUsphere [preprint], https://doi.org/10.5194/egusphere-2024-115, 2024.

Teuling, A. J. and Hoek van Dijke, A. J.: Forest age and water yield, Nature, 578, E16-E18, https://doi.org/10.1038/s41586-020-1941-5, 2020.

Teuling, A. J., de Badts, E. A. G., Jansen, F. A., Fuchs, R., Buitink, J., Hoek van Dijke, A. J., and Sterling, S. M.: Climate change, reforestation/afforestation, and urbanization impacts on evapotranspiration and streamflow in Europe, Hydrol. Earth Syst. Sci., 23, 3631–3652, https://doi.org/10.5194/hess-23-3631-2019, 2019.

Tixeront, J.: Prévision des apports des cours d'eau, Publication de l'Association internationale d'hydrologie scientifique, 63, 118–126, http://pascal-francis.inist.fr/vibad/index.php?action=getRecordDetail&idt=19271864 (last access: 24 August 2024), 1964.

Tong, R., Parajka, J., Széles, B., Greimeister-Pfeil, I., Vreugdenhil, M., Komma, J., Valent, P., and Blöschl, G.: The value of satellite soil moisture and snow cover data for the transfer of hydrological model parameters to ungauged sites, Hydrol. Earth Syst. Sci., 26, 1779–1799, https://doi.org/10.5194/hess-26-1779-2022, 2022.

Van der Velde, Y., Vercauteren, N., Jaramillo, F., Dekker, S. C., Destouni, G., and Lyon, S. W.: Exploring hydroclimatic change disparity via the Budyko framework, Hydrol. Process., 28, 4110–4118, https://doi.org/10.1002/hyp.9949, 2014.

Van Loon, A. F., Stahl, K., Di Baldassarre, G., Clark, J., Rangecroft, S., Wanders, N., Gleeson, T., Van Dijk, A. I. J. M., Tallaksen, L. M., Hannaford, J., Uijlenhoet, R., Teuling, A. J., Hannah, D. M., Sheffield, J., Svoboda, M., Verbeiren, B., Wagener, T., and Van Lanen, H. A. J.: Drought in a human-modified world: reframing drought definitions, understanding, and analysis approaches, Hydrol. Earth Syst. Sci., 20, 3631–3650, https://doi.org/10.5194/hess-20-3631-2016, 2016.

van Oorschot, F., van der Ent, R. J., Hrachowitz, M., and Alessandri, A.: Climate-controlled root zone parameters show potential to improve water flux simulations by land surface models, Earth Syst. Dynam., 12, 725–743, https://doi.org/10.5194/esd-12-725-2021, 2021.

van Oorschot, F., van der Ent, R. J., Alessandri, A., and Hrachowitz, M.: Influence of irrigation on root zone storage capacity estimation, Hydrol. Earth Syst. Sci., 28, 2313–2328, https://doi.org/10.5194/hess-28-2313-2024, 2024.

Verdin, K. L.: Hydrologic Derivatives for Modeling and Applications (HDMA) database: U. S. Geological Survey data release, U.S. Geological Survey data release, https://doi.org/10.5066/F7S180ZP, 2017.

Wagener, T., McIntyre, N., Lees, M., Wheater, H., and Gupta, H.: Towards reduced uncertainty in conceptual rainfall-runoff modelling: Dynamic identifiability analysis, Hydrol. Process., 17, 455–476, https://doi.org/10.1002/hyp.1135, 2003.

Wang, S. and Hrachowitz, M.: Data and code underlying the publication: Multi-decadal fluctuations in root zone storage capacity through vegetation adaptation to hydroclimatic variability has minor effects on the hydrological response in the Neckar basin, Germany, 4TU.ResearchData [code and data set], https://doi.org/10.4121/922d30de-a26b-4c81-8644-ad036182239c, last access: 27 August 2024.

Wang, S., Hrachowitz, M., Schoups, G., and Stumpp, C.: Stable water isotopes and tritium tracers tell the same tale: no evidence for underestimation of catchment transit times inferred by stable

isotopes in StorAge Selection (SAS)-function models, Hydrol. Earth Syst. Sci., 27, 3083–3114, https://doi.org/10.5194/hess-27-3083-2023, 2023.

Wang-Erlandsson, L., Bastiaanssen, W. G. M., Gao, H., Jägermeyr, J., Senay, G. B., van Dijk, A. I. J. M., Guerschman, J. P., Keys, P. W., Gordon, L. J., and Savenije, H. H. G.: Global root zone storage capacity from satellite-based evaporation, Hydrol. Earth Syst. Sci., 20, 1459–1481, https://doi.org/10.5194/hess-20-1459-2016, 2016.

Yang, Y., Zhu, Q., Peng, C., Wang, H., Xue, W., Lin, G., Wen, Z., Chang, J., Wang, M., and Liu, G.: A novel approach for modelling vegetation distributions and analysing vegetation sensitivity through trait-climate relationships in China, Sci. Rep.-UK, 6, 24110, https://doi.org/10.1038/srep24110, 2016.

Zhang, L., Dawes, W., and Walker, G.: Response of mean annual evapotranspiration to vegetation changes at catchment scale, Water Resour. Res., 37, 701–708, https://doi.org/10.1029/2000WR900325, 2001.

Zhang, L., Hickel, K., Dawes, W. R., Chiew, F. H., Western, A. W., and Briggs, P. R.: A rational function approach for estimating mean annual evapotranspiration, Water Resour. Res., 40, W02502, https://doi.org/10.1029/2003WR002710, 2004.

Zhou, S., Yu, B., Huang, Y., and Wang, G.: The complementary relationship and generation of the Budyko functions, Geophys. Res. Lett., 42, 1781–1790, https://doi.org/10.1002/2015GL063511, 2015.